AD-A062 063 WESTINGHOUSE RESEARCH AND DEVELOPMENT CENTER PITTSBU--ETC F/G 13/8
INVESTIGATION OF WELD POOL STRUCTURE AND PROPERTY CONTROL IN PU--ETC(U)
OCT 78 G M ECER N00014-77-C-0596
UNCLASSIFIED 78-9D4-PULSE-R1 NL

1 OF 1
ADA
062063

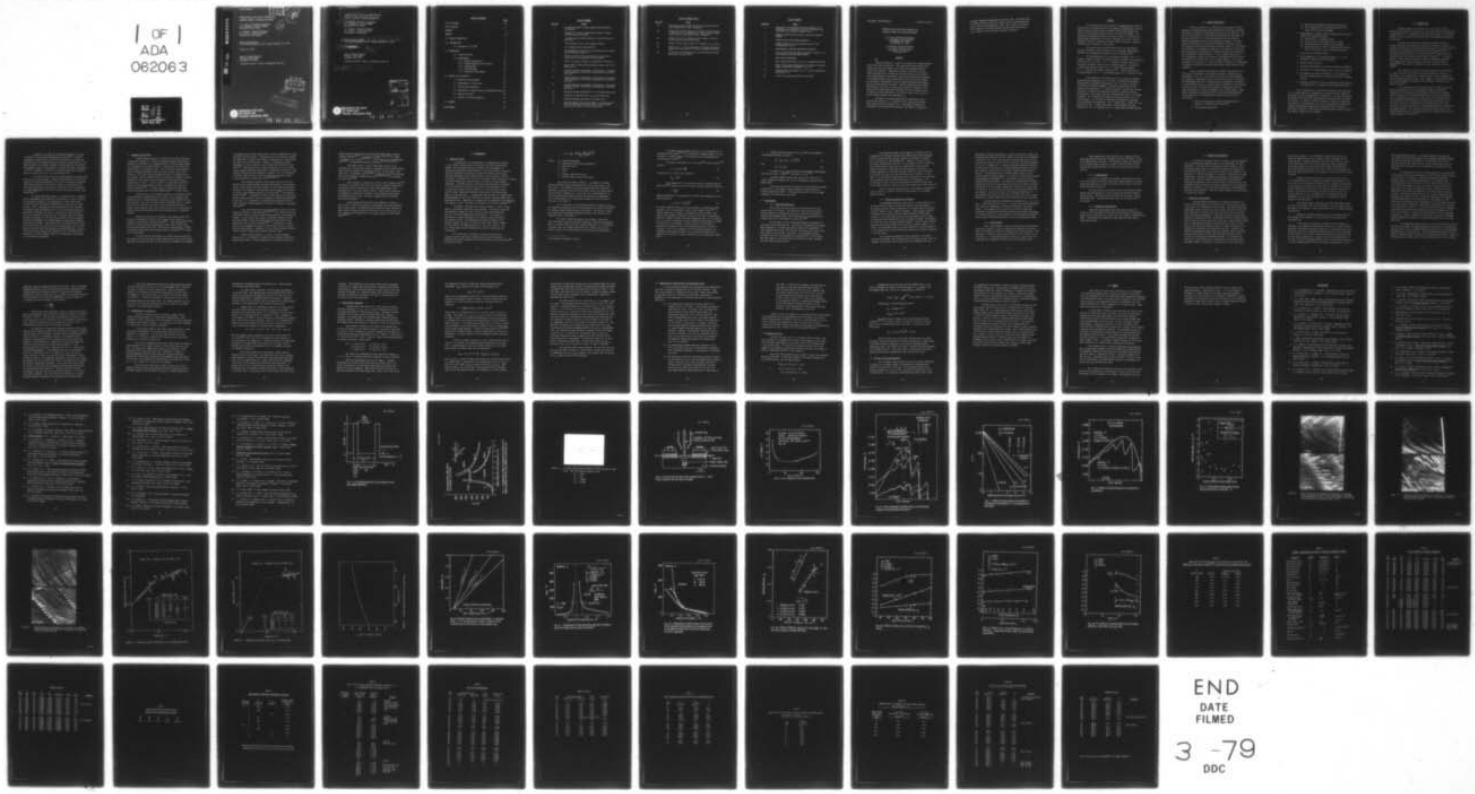

END
DATE
FILMED
3 -79
DDC

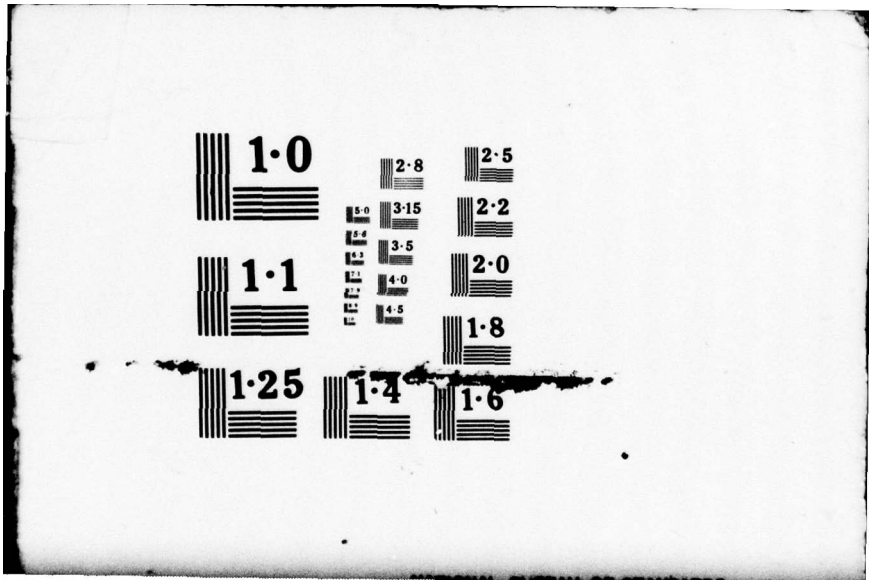
1·0
1·1
1·25
1·4
1·6
1·8
2·0
2·2
2·5
2·8
3·15
3·5
4·0
4·5
5·0

78-9D4-PULSE-R1

LEVEL II

INVESTIGATION OF WELD POOL STRUCTURE AND PROPERTY CONTROL IN PULSED ARC WELDING

G. M. Ecer - Principal Investigator
G. G. Lessmann - Project Manager
Westinghouse R&D Center

A. Tzavaras - Visiting Professor
H. D. Brody - Project Director
University of Pittsburgh

Annual Progress Report
For Period September 15, 1977 through September 14, 1978

October 31, 1978

Office of Naval Research
800 North Quincy Road
Arlington, VA 22217

Scientific Officer: Bruce A. MacDonald (Code 471)

Westinghouse R&D Center
1310 Beulah Road
Pittsburgh, Pennsylvania 15235

(14) 78-9D4-PULSE-R1

(6) INVESTIGATION OF WELD POOL STRUCTURE AND PROPERTY CONTROL IN PULSED ARC WELDING.

(10) G. M. Ecer - Principal Investigator
G. G. Lessmann - Project Manager
Westinghouse R&D Center

A. Tzavaras - Visiting Professor
H. D. Brody - Project Director
University of Pittsburgh

(9) Annual Progress Report, 15 Sep 77-14 Sep 78,
For Period September 15, 1977 through September 14, 1978

(11) 31 Oct[redacted]978

(12) 79 p.

Office of Naval Research
800 North Quincy Road
Arlington, VA 22217

Scientific Officer: Bruce A. MacDonald (Code 471)

(15) N00014-77-C-0596

Westinghouse R&D Center
1310 Beulah Road
Pittsburgh, Pennsylvania 15235

TABLE OF CONTENTS

LIST OF FIGURES

LIST OF FIGURES (cont.)

LIST OF TABLES

R&D Report 78-9D4-PULSE-R1 October 31, 1978

INVESTIGATION OF WELD POOL STRUCTURE AND PROPERTY CONTROL IN PULSED ARC WELDING

G. M. Ecer, Principal Investigator
G. G. Lessmann, Project Manager
Westinghouse R&D Center
Pittsburgh, PA 15235

A. Tzavaras, Visiting Professor
H. D. Brody, Project Director
University of Pittsburgh
Pittsburgh, PA

ABSTRACT

Initial findings on a study of the pulsed arc welding solidification structures are reported. Full penetration pulsed current gas tungsten arc welds in Fe-26Ni alloy sheets were dimensionally and structurally analyzed. Temperature profiles at various locations of several weldments were recorded and weld pool kinetics were studied using cinematography, conventional and scanning electron metallography. A two dimensional heat flow computer model of the pulsed arc welding was developed. Experimental data were comparatively analyzed against the early predictions of the model. Thermal conductivity and thermal diffusivity of the alloy, as well as heat transfer efficiency of the pulsed current GTAW process were estimated for use as computer input. In addition, melting efficiency of the process under various sets of pulsed welding variables was determined.

The effort so far has established an experimental and a computational approach for studying the full penetration welding under pulsed current gas tungsten arc. The agreement between the experimental and calculated data was good with regard to temperature

profiles, temperature gradients and the G/R ratio. Additional work is needed to further refine the computer model in estimating local growth rates and solidification times. Heat transfer and melting efficiencies of the PC-GTAW process improved with increasing arc travel speed, low pulse current and total arc energy.

FORWARD

This progress report was prepared by the Westinghouse Electric Corporation in collaboration with the University of Pittsburgh, under the Office of Naval Research Contract N00014-77-C0596, "Investigation of Weld Pool Structure and Property Control in Pulsed Arc Welding". The program was administered under the technical direction of the Office of Naval Research Department of the Navy, Arlington, VA, with Dr. Bruce A. MacDonald (Code 471) serving as the ONR Scientific Officer in charge of inspection and acceptance of the program.

The project work is being carried out by the Westinghouse Electric Corporation with the University of Pittsburgh, Metallurgical and Materials Engineering Department acting as a subcontractor.

The Westinghouse part of the program is managed by Mr. G. G. Lessmann, Manager of Metals Joining and Metals Processing, and technically directed by Dr. G. M. Ecer. Dr. R. P. Simpson, initially involved in the project planning, has acted in an advisory capacity. Significant contributions were also made by Mr. D. F. Baker (vacuum melting), Mr. A. J. Heim (sheet rolling, annealing), Mr. J. Rogy (welding set-up and measurements), Mr. J. P. Yex (metallography), Mr. R. Kuznicki (x-ray),

The University of Pittsburgh part of the program is managed and technically directed by Dr. H. D. Brody, Professor and Chairman of Metallurgical and Materials Engineering. Dr. S. A. David, initially involved in the program planning, is currently employed by the Oak Ridge National Laboratory. Dr. David has served in an advisory capacity. Professor A. Tzavaras of Aristotelian University, Salonica, Greece, participated in the project from June through October 1978 as a visiting professor. Mr. M. Vassilaros prepared the computer model as part of a course project. Mr. Tri Dinh has modified the program and performed the correlations with Experiment. Mr. A. Gokhale, Ms. L. Smith, Ms. M. A. Krenicky, and Mr. J. Gasper have helped in metallographic specimen preparation. Mr. G. M. McManur and Dr. R. Sinha aided with SEM analysis.

1.0 PROJECT DESCRIPTION

Current pulsation in arc welding can be tailored to produce periodically changing cooling rates along the weld seam thus affecting the primary and secondary solidification pattern of the weld pool. The mode of solidification, on the other hand, substantially determines the weld metal properties, by influencing grain size and orientation, phases precipitated as well as the segregation processes. The wide range of solidification rates which are possible with pulsed current arc welding processes make them highly desirable methods for controlling weld properties. Development of methods of weld structure control can product significant improvements in weldment properties and reliability with considerable economic benefits. In this regard, this project, "An Investigation of Weld Pool Structure and Property Control in Pulsed Arc Welding" was funded by the Office of Naval Research. The overall objective of the program is to control weldment properties by establishing relationships between the properties and pulsed current welding process variables.

Under the ONR Contract N00014-77-C-0596, work began early in 1978, with the University of Pittsburgh acting as a subcontractor to Westinghouse. The first year's effort was focused on the development of a predictive mathematical model of pulsed arc welding of thin sheets (two-dimensional heat flow), establishing the experimental techniques to develop physical data to correlate process variables to weld solidification structure, and comparative analysis of experimental data and model predictions for further refinement of the computer model. These efforts involved the following specific tasks on which Westinghouse and the University of Pittsburgh have worked either separately or concurrently.

1. Review of literature on pulsed current welding with emphasis on solidification related work.
2. Weld specimen preparation:

(a) Model alloy (Fe-26% Ni) melting and fabrication,
(b) Heat treatment and x-ray characterization of the model alloy thin sheet specimens.

3. Establishment of pulsed current welding procedure for thin sheets (full penetration welds):
   (a) Construction of a welding fixture,
   (b) Selection of electrode shape and arc length,
   (c) Characterization of pulsed current waveforms,
   (d) Characterization of the arc voltage-current relationship for the pulsed current welding power supply.
4. Preparation of PC-GTAW specimens.
5. Macro examination of the welded specimens, i.e., bead dimensions, grain and ripple morphology.
6. Microstructural analysis.
7. Temperature measurements at various locations of weldments.
8. Initiation of a cinematographic study of weld pool kinetics.
9. Development and initial refinement of a two dimensional heat flow computer model of the pulsed current arc welding process.
10. Comparative analysis of results, experimental and predicted, and preparation of a progress report covering 1978 work.

In the coming years, efforts will be focused on the refinement of the computer model to accommodate more realistic welding conditions determined through experiments and the extension of both the experimental and modeling work into three dimensional heat flow situations in pulsed arc welding. In addition, effects of pulsed arc welding on segregation processes will be explored with the intent of studying hot cracking and hydrogen embrittlement problems under pulsed heat input conditions. Predictive capability of the refined model will then be tested on several more complex commercial alloy systems.

2.0 INTRODUCTION

Weldment quality, for the most part, is a function of the solidification process in the weld pool. All three types of solidification related defects, i.e., segregation, inclusions and porosity, are directly related to the structure of the weld which in turn influences the quality of the joint.

Although the literature abounds with references relating welding procedures and techniques to mechanical properties, relatively few deal with the study of the solidification structure of welds per se[1-4]. Naturally, even fewer papers deal with methods for controlling the solidification structure and the ensuing problems[5-8], and more so for particular types of welding such as pulsed arc welding[9]. It appears, however, that in eastern countries at least two research groups have been working with the solidification structures produced in pulsed welding[10,11] and claims of controls for these structures have been made[11].

The technique of pulsed arc welding combines the good features of a high current such as good penetration and steady arc with the advantages of low currents such as smoother bead, no burn throughs and better energy and material usage. Thus a number of tough welding problems have been successfully treated with this technique, but mostly on an empirical basis[9].

It is believed that this technique can be further refined and improved substantially if the relationship between the operating parameters and the resulting solidification structure is established. This is because of the increased possibilities for control variations that this technique introduces. In other words this technique offers a new potential for controlling the solidification conditions in the weld pool; but the new potential can be exploited only if the basic processes occurring in the weld pool under pulsed welding are researched and understood well. For instance, effective grain size control can improve substantially not only the sturcture but, through structure, the cracking behavior of the weld[12].

In general, the larger the individual dendrites the larger the defects in the related solidification structure[13]. The main advantage of controlling the solidification structure of a weld with physical rather than chemical means is the general applicability of the method without the problems a chemical refining agent may cause later (brittleness because of precipitation, selective corrosion, segregation, etc.)[14]. Therefore, a weld with a refined solidification structure, achieved by physical means, is a very desirable weld.

It is clear, that in order to achieve desirable solidification structures in pulsed welding, a detailed understanding of the relation between the operating parameters, such as the current-time profile and other characteristics of the applied currents, on one hand and the resulting solidification structures on the other, must be established. The present knowledge in this area is rather sketchy and at best, semi-qualitative[15].

In approaching this problem, it was realized that a combined effort, experimental and analytical, was necessary in order to produce the information needed for the development of a model which would correlate process variables and solidification structures for pulsed welding. Thus, a mathematical model simulating heat flow in pulsed arc welding and an experimental set-up for actual pulsed welding were developed to implement this effort. The object of this dual effort was to make possible for each approach to mutually assist and improve the other continually so that the best information could be produced towards the development of a general model, as realistic as possible, for pulsed arc welding. The research effort expanded within the first year of the project is reported in the following pages, after a brief review of pulsed current gas tungsten arc welding (PC-GTAW). Portions of the first year's results were presented at the 1978 AIME-TMS Fall Meeting in St. Louis, Missouri, and will be submitted for publication in the conference proceedings.

2.1 Background on PC-GTAW

Pulsed current welding is a relatively new process variation that has been applied to a variety of welding processes including gas tungsten arc, gas metal arc, shielded metal arc, electron beam, plasma arc, submerged arc, and laser welding. Literature on the subject has already grown to an impressive size. Over 250 articles have appeared, mainly in Russian journals, within the last 15 years. Much of the interest in the pulsed current welding has been in its application to GTA welding. This is reflected both in the number of technical articles published on the subject and in the number of PC-GTA welding power supplies sold in the U.S. Close to 45% of all GTA power sources sold within the last year by Hobart Brothers, for example, had built-in pulsing capability[16]. A definite surge in sales of PC-GTAW power supplies was experienced by another manufacturer[17] in recent years.

Pulsed current, in GTA welding, produces a continuously welded seam consisting of overlapping arc spot welds. In its simplest form welding current is switched between a high level that produces the arc-spot weld and a low level that only serves to maintain the arc. Figure 1 describes the terms that are often used in process descriptions of pulsed current welding. Most often, pulsing occurs at the same polarity; however, there are variations that utilize current waves of reversible polarity.

Because the weld pool is allowed to cool between pulses, and the heat is dissipated in the work, the effect of heat build-up or disparity in heat sink is largely overcome[18]. Some investigators[19-21], therefore, report much better penetration control with pulsed current GTA than with steady current GTA. Slag build-up problem which is common in welding certain steels like maraging steels is eliminated[18] as well, for the same reason.

In steady current GTA welding, the thermal surplus between the heat input due to the arc and the heat removed by the work causes melting. Variations in either heat input or heat sink lead to changes in the degree

of melting, which may then result either in lack of penetration or drop through of the molten pool. A skilled operator can partially overcome this difficulty, in manual GTA welding, by manupulation of the welding gun and/or the cold filler wire. However, in mechanized welding, variations in the heat balance lead to significant variations in the joint[18]. This last factor is largely avoided by the use of pulsed current welding techniques which exhibit considerable tolerance to such external variables as joint geometry, clamping or fit up, differences in thermal conductivities of metals being joined and other factors causing variation in thermal heat sink[18,20,22,23].

The operating tolerance arises largely from the fact that during the low current periods, the weld pool formed by the preceding pulse of high current solidifies rapidly, the heat being dissipated in the mass of the weldment. Each subsequent pulse starts on relatively cool plate, thus minimizing effects of heat buildup[22] and disparity in heat sink[18]. Consequently, pulsed current welding is particularly suited to mechanization, and can be automated by having some parameter of the weld, i.e., penetration, automatically monitored and used to adjust the pulse current amplitude or duration to maintain a consistent weld bead[18].

For a given penetration weld using pulsed current and conventional GTA welding, it has been shown[20,24-27] that the heat input is consistently lower for pulsed current welding than for conventional GTA welding. In the former case, energy is delivered through the anode spot more rapidly so that local melting occurs before there is any significant loss of heat by conduction[28]. Consequently, a larger portion of the workpiece is melted in PC-GTA than in GTA if the heat input is held constant. Conversely, if the volume of workpiece melted is held constant, PC-GTA should require less heat input.

Almost without exception, to achieve the best weldment properties, it is preferable to accomplish the necessary melting with minimum energy input. PC-GTA welding, with its lower heat input and

higher intensity heat source than conventional GTAW leads to reduced residual stresses[29-31], structural refinement[10,11,32-35], higher resistance to hot cracking[33,35-37], reduced width of the heat-affected zone[19,35] and improved mechanical properties[11,24,29,32,33,35].

The higher level of current (high pulse current) can be typically two or three times greater in magnitude than the steady current which could be required of conventional GTA for the same joint. This means that a considerably stiffer[38,39] welding arc forms during pulsing which in turn results in deeper penetration[20,31,40,41] and increased arc stability[42-45].

Other benefits of pulsing the current in GTA welding include[46] a reduction in operator skill level and fatigue in manual welding due to the lowered need for electrode and filler metal manipulation, and minimization of foot pedal current control. Pulse current control may be regarded as an added tool available to the welding operator which will extend his skill level, and assist significantly in achieving reproducible weldments.

Pulsed Current-GTA process has been employed in welding a wide variety of materials and material thicknesses that range from foil gage to heavy plates. Considerable applications have been reported for small diameter tubing and piping in both the U.S.S.R. and the U.S.; in fact, pipe and tube welding is by far the most popular of the PC-GTAW usage[16-17].

3.0 METHODOLOGY

3.1 Analytical Study

As explained in the Introduction, in approaching the problem it was decided to develop both an analytical tool and an experimental method. The analytical approach provided for the development of a mathematical model which would simulate, in the first phase of the study, heat flow conditions encountered in pulsed arc welding of thin sheets. The model developed, as most similar models, uses the method of finite differences to describe heat flow in two directions from a continuous or pulsing heat source moving with constant speed on a plane with known thermal properties. The model utilizes a matrix with approximately 500 elements. It can be used with and without heat losses to the environment and it can take into account convection effects in the liquid phase, latent heat of fusion, temperature dependent conductivity, heat capacity and density of the base metal. In simulations reported here, all elements have been considered to be at 25°C, when the run starts; although preheat may be simulated as well. Computation is stopped when the temperature has stabilized with respect to time. The model is described in more detail elsewhere[47].

In summary, the model uses a digital computer to solve a large number of relatively simple heat flow equations. The equations describe the temperature change of a small volume of metal experiencing heat flow to or from the neighboring volume elements. Each element is described by a single temperature of an assumed concentrated mass at the element's center. The temperature differences between all the adjacent elements are used to compute the heat flows between elements and thus predict the temperatures after a given time interval. The use of small time intervals minimizes any errors in predicting the temperatures.

As a first test of the model, the model was applied to continuous rather than pulsed welding and the temperature profiles computed with it were compared with profiles based on the Adams equation[48] which is as follows:

$$T - T_o = \frac{q}{4k} \cdot \frac{\exp\left[m - (m^2 + n^2)^{1/2}\right]}{(m^2 + n^2)^{1/2}}$$

where: T_o = initial temperature

T = temperature above initial temperature

q = heat input rate

$m = vx/2x$

$n = vR/2$

x = distance behind heat source

R = distance away from heat source path

The results are shown in Figure 2. As expected, the Adams equation predicts higher temperatures than the new model close to the heat source. The difference increases exponentially with decreasing distance to the point directly below the heat source. The Adams equation yields infinite temperature for this point; but at approximately 2 cm from this point the difference between the two curves is negligible. What is more important, the temperature gradients for the two sets of curves are very similar.

As a second test, the maximum bead width for continuous welds was computed and compared with the results based on the Wells' equation[49] for various electrode velocities and heat inputs. The two sets of data were found in good agreement (maximum difference less than 10% of the predicted value -- see Table 1).

To further refine the accuracy of the model, a particular effort was made to determine reliable estimates of the various parameters used in the model such as the heat transfer efficiency (μ_1), the melting efficiency (μ_2), the thermal conductivity (k), density (ρ), and the specific heat C_p of the base material used during this investigation.*

---

* All symbols are defined in Table 2.

Calorimetrically determined values of μ_1 are reported only for non-melting work pieces[50,51] and theoretical estimates appear to be too difficult to attempt because of the complexity and interdependence of the processes involved[52].

Indirectly an estimate of μ_1 can be made[53] based on Wells'[49] equation

$$q = 8k\ T_m\ (\frac{1}{5} + \frac{vd}{4\alpha}) \tag{1}$$

from which the net input can be computed

$$H_{net} = \frac{q \cdot \delta}{v} \tag{2}$$

Good estimates of k can be derived based on published experimental data[54] which in turn can be used to estimate thermal diffusivity.

$$\alpha = \frac{k}{C_p \cdot \rho} \tag{3}$$

Reliable estimates of the variations of density with temperature can be made according to

$$\rho = \rho_o \left[1 + 3\ \frac{L - L_o}{L_o}\right]^{-1} \tag{4}$$

for linear expansion from L_o to L corresponding to temperature change between T_o and T and published linear thermal expansion data[55]. A similar approach can be made in estimating C_p values; however, this appears to be somewhat problematic because of the lack of experimental data above 1200°K to support linearity assumptions made for the function $\ln C_p = f\ (\ln T)$ on the basis of data available between 300°K and 1200°K. This problem is not expected to affect seriously the information produced by the model, as far as the thermal diffusivity values are concerned. As it will be apparent in the following paragraph, the temperature distribution profiles show considerable insensitivity to substantial variations of thermal diffusivity if the temperature exceeds 500°K.

Grossly inaccurate values for C_p may affect the estimate of the melting efficiency μ_2 because

$$H_m = (H_T + H_\ell)\ \rho \cdot \delta \cdot \frac{d_f + d_b}{2} \qquad (5)$$

and

$$H_T = \int_o^T C_p dT \qquad (6)$$

The value of H_ℓ can be estimated using published thermodynamic data such as those of Oriani[56] and Zellers, et.al.[57].

The model assumes further that the heat of fusion (H_ℓ) is evenly released or absorbed over the 25°C temperature range of the two phase region.

Convection effects were accounted for by increasing the thermal conductivity of any element having a temperature greater than the liquidus temperature 1468°C. A multiplication factor of 25 was judged reasonable for this phase of the study.

3.2 Experimental

3.2.1 Material Preparation

The Fe-26Ni alloy was selected as the model alloy for the initial phase of this work. The selection of this alloy was based on ease with which its solidification structure could be identified by ordinary metallographic means, and also because of the availability of previous data over a wide range of cooling rates[58].

The base metal for the welding experiments was prepared in a laboratory vacuum induction heat. The heat was deoxidized with graphite. Minor additions of Si and Mn were made to improve hot workability. A slab weighing about 30 lbs. (13.6 kg) was cast under vacuum and hot and cold rolled to various sheet thicknesses. An intermediate anneal, 4h-2150°F (1177°C) in dry hydrogen, was applied prior to cold rolling. The total amount of cold work was kept to 20% in all cases. Rolling direction was also kept constant.

It was hoped that with a final anneal of 4h-2150°F (1177°C) followed by slow cooling a cube-on-face texture with a <100> direction in the rolling direction could be promoted as described by Savage[4] for the processing of the Fe-49Ni alloy. However, a series of back reflection Laue patterns taken over a 4 cm distance at 0.5 cm intervals, and a diffractometer trace of the as annealed metal showed totally random orientation of martensite and small amounts of austenite. A similar examination of the weld zone back reflection along a line half way between the center line and the fusion line of weld No. J-7 (see Table 3 for conditions) indicated some (211) preference in the martensite and pronounced preferred (220) orientation of the austenite. The diffractometer trace of the weld zone showed an abnormally high count on the (200) reflection indicating preferred orientation in this direction.

Finally, the base metal produced for the present investigation took the form of a 0.032 in. (0.081 cm) thick sheet, of an analysis shown in Table 4.

3.2.2 *Welding Equipment and Procedure*

A programmable GTAW power supply with a current range of up to 150 amps (Astro-Arc Model CA-150-TS) was used for the investigation. The machine controls allowed adjustments of the high pulse and low pulse currents (Figure 1) with 1 ampere increments. Their duration could be individually set between 0.005 and 0.999 seconds with 0.001 second intervals. The travel speed was controlled separately and was tested for uniformity and repeatability prior to making the welds. All welding was done with direct current electrode negative. Pulsed current waveform remained nearly square shaped within the pulse frequency range of 1 to 48 Hz. An oscilloscope trace of a typical waveform is shown in Figure 3. It was obtained from a 100 mv-400A shunt placed near the ground connection of the weld table.

The following parameters were kept constant in all welds: electrode composition, size and shape were W + 2% ThO_2, 1/8 in. (0.32 cm) diameter, 30° included vertex angle with 0.04 cm diameter flat tip;

100% argon as shield gas flowing at a rate of 40 cfh (18.9 1/min) from around the electrode and 4 cfh (1.9 1/min) to the back of the weldment; arc gap of 0.1 in. (0.25 cm); electrode stick-out from the cup 0.5 in. (1.25 cm) and from the collet 1.16 in. (2.95 cm); base metal thickness of 0.032 in. (0.08128 cm). In addition specimen clamp down procedure and the relative positions of the fixture/specimen/welding torch were kept identical in all cases by utilizing a welding fixture shown in Figure 4. The specimen could be clamped between Teflon strips to prevent distortion during welding. A constant arc length was maintained during welding by adjustment of a flat platform plate on which the aluminum fixture was placed. Arc stability was maintained by welding towards the ground connection which was bolted on the edge of the base metal sheet in a way to assure symmetrical conduction of current away from the weld. For each run a new location for the ground connection was selected. The use of Teflon, with a thermal conductivity of approximately 250 times less than that of Fe-26Ni alloy, was to assure minimal heat exchange between the fixture and the base metal specimen.

Welding variables independently evaluated were i_p, i_b, t_p, t_b and v. Other variables such t_p/t_b, f, P and H could also be evaluated since these were dependent on the former variables as indicated in Table 2. Arc voltage-current relation for the power supply was determined using the above described materials and welding conditions. It is shown in Figure 5, and is similar to those reported by Savage[59]. Table 3 gives the PC-GTAW parameters used for the experimental welds.

3.2.3 Metallography

From a large number of welds produced during the experiments described in Table 3, a series of samples were selected from various sites in the base metal after the welding process had stabilized. From this group, a series of samples was selected to cover a matrix of two variables, i.e., increasing high pulse current (i_p) (heat input) and increasing pitch (distance traveled for one full pulsing cycle).

These samples were first studied with a scanning electron microscope and then sectioned, polished and etched with Nital to study their solidification structure. The SEM study covered the morphology of the solidification structure in relief in both the upper (front) and the lower (back) surfaces of the weld and selective x-ray micro-analysis.

3.2.4 Cinematography

In order to understand the processes occurring in the weld pool during pulsed arc welding, high speed cinematography was utilized during one welding run to record the motion of the liquid, the solid-liquid interface and the arc.

The film produced was analyzed using a professional editing machine with the capacity to record lapsing time and frame sequence electronically. Both frame by frame analysis and viewing at various speeds were made. Further films will be made in the second year of the project.

3.2.5 Temperature Measurements

Temperature measurements were taken using at least four 0.008 in. (0.02 cm) diameter Pt-Pt 10% Rh thermocouples strategically placed close to and within the fusion zone for a number of characteristic welds. The results were recorded on light sensitive paper using a high speed recorder.

4.0 RESULTS AND DISCUSSION

In this first progress report, a portion of the data obtained will be presented with emphasis placed on the methodology and their reliability. More data will be presented in future reports. This is because the present report is written while some of the results are still being obtained and, in some cases, are not fully evaluated. As mentioned in a previous paragraph, the problem of establishing reliable thermal data on pulsed arc welding was approached experimentally and analytically. The dual approach adopted helped in estimating and reducing the magnitude of the errors introduced, either because of the assumptions made in carrying out various computations in the analytical approach or because of the difficulties encountered in performing and monitoring the experiments. This will become apparent in the discussion of results that follows.

4.1 Temperature Measurements

The experimental measurements of temperature presented an unusual difficulty because of the small size of the weld bead relative to the size of the thermocouple's hot junction. This makes temperature measurements within the weld pool particularly difficult because it is nearly impossible to pinpoint the exact location in which the thermocouple was sensing temperatures. Additional difficulties result from alloying and induction effects, particularly for sites in which there is direct contact of the hot junction with the melt. These problems persist even for thermocouples placed in sites which do not come in contact with the melt during the welding process, but they are expected to be somehwat less severe than in sites within the melt. Therefore, the temperature measurements made outside the weld bead can be considered as more reliable than the ones within the bead and therefore more suitable for evaluating the mathematical model. For instance, the location of a hot junction can be determined with an accuracy which approaches 2/100 of a centimeter, and as long as it does not come in

contact with the melt, it is reasonable to assume that the site in which the temperature data are recorded is well established for the entire process. Alloying effects are also much less severe for sites in the base metal that do not reach liquidus or higher temperatures for obvious reasons; and as the sites that remain solid during the entire process are more remote from the arc (than the sites within the melt) the induction effects are also expected to be less severe for these locations.

Another problem, particular to the pulsed welding process, is the determination of the temperature gradients around the arc. The heat flow is not continuous and, therefore, the temperature distribution is not constant, but varies with time within the pulsing cycle with the current-time profile of the pulse cycle and the distance from the heat source. Additional difficulties are caused from the fact that the liquid around the arc is not stagnant and its flow patterns are not established in most cases, but even more so for pulsed arc welding because of the Lenz effect.

Thus reliable direct temperature gradient measurements within the bead of relatively small size welds appear to be very difficult and the results are expected to have considerable errors of unknown magnitude and direction.

Temperature gradient measurements in the solid base metal are more reliable and a sample of two such cases will be presented and discussed here.

In the case of continuous arc welding, once the process is stabilized, the temperature distribution around the arc remains constant. Therefore, the maximum temperature gradient for a particular site in the solid base metal can be established relatively easy (it will occur when the heat source is at a certain established distance and direction from the site under consideration). However, this is not necessarily so in the case of pulsed arc welding simply because at the time the heat source is at the minimum distance from the site under consideration, it may or

may not be emitting any heat. As discussed earlier, the magnitude, the time it occurs and the direction of the maximum temperature gradient for a site in the solid base metal, is a function not only of the distance from the heat source but also of the current-time profile of the pulse and the velocity of the arc relative to the velocity of the heat wave.

An analysis which takes all these parameters into consideration has been made and it will be presented in the next annual report; however, in some cases, it is possible to estimate the maximum temperature gradients close to the weld bead much easier on a different basis. If the time period for one full pulse cycle is a small fraction (1/5 to 1/4) of the time needed for the arc to travel a distance equal to the long axis of the liquid pool, then there is only one major heat wave sweeping the sites under consideration, in the base metal but close to the bead. This wave, however, does not have a smooth temperature-time profile but a serrated one with a series of fluctuations corresponding to ON-OFF time periods of the high pulse arc, (see Figure 6). The smaller the forementioned ratio, the smoother the time-temperature profile of the heat wave as indicated by temperature fluctuations (ΔT) predicted by the model shown in Figure 7. This has also been observed by comparing temperature-time profiles for experimental welds, for example welds J-4 and J-7 as in Figure 8. Based on the above analysis and the data shown in Figures 6, 7 and 8, a method can be developed to estimate the maximum possible temperature gradient at the weld bead boundary and on the base metal side.

If a temperature-time profile at a site in the base metal near the weld bead is recorded, the maximum temperature fluctuation is recorded when the heat source is at the minimum distance from the site of the thermocouple. This means that at this time (i.e., when the maximum fluctuation in temperature is recorded) there is liquid at the nearest possible point. Stated in a different way, the nearest point on the weld fusion line is at the solidus

temperature when the maximum fluctuation is recorded. Thus, the maximum temperature gradient at the weld bead boundary can be expressed as the maximum temperature difference between the solidus and the minimum temperature at the recording site (ΔT_{max}) divided by the minimum distance of the recording site to the weld bead boundary (ℓ_{min}) provided the recording site is close enough to the weld bead.

$$G_S = \frac{T_{max}}{\ell_{min}}$$

Based on the above reasoning, a series of temperature measurements from experimental welds have been evaluated and some of the results are shown in Table 5. The data show the temperature gradients in the solid side (G_S) and on the liquid side (G_L) of the bead-base metal interface. However, the data on G_L must be used with caution because of forementioned possible errors in temperature recording.

As expected, the temperature gradients measured in this study diminish with increasing distance from the weld (the temperature distance curve is known to have a negative derivative with a decreasing absolute value for lower T). Unexpectedly, however, a considerable drop in temperature (approximately 70°K) was measured at the very weld bead boundary. Stated differently a temperature at least 70°K higher than the solidus was recorded at the solid-liquid interface or over a distance which must be equal or small than 0.02 cm, i.e., the accuracy of distance measurements. This temperature drop can be explained if there is a considerable drop in temperature near the solid-liquid interface, at least, for the alloy under consideration. Among the data of Table 5, the temperature gradients in the solid (G_S) should be considered as more accurate than those in the liquid (G_L) for reasons discussed in the previous paragraph. On the other hand, the accuracy of the data in the solid (G_S) increases with decreasing distance from the weld bead-base metal interface. Therefore, the most accurate measurement is the one made over the shortest distance, i.e., 0.43 mm and yielded 1030°K/mm. This value should be considered as a minimum possible temperature gradient at the interface (on the solid side).

The liquid temperature gradients for reasons explained already are only indicative and in view of the cinematography data can hardly be used as a basis for further computations. They are indicative, however, of low temperature gradients persisting in the bulk liquid, as compared to those in the solid, as a result of the intense flow in the weld pool. It should be emphasized, particularly in view of the measurement made near the fusion line, low thermal gradients can only be true in the bulk liquid phase and they do not apply in the liquid boundary at the liquid-solid interface.

4.2 Measurements of Growth Rate

The most convenient method for measuring growth rates in pulsed and welding appears to be high speed cinematography. This technique of direct observation, when used properly, can yield acceptable information with regard to growth. Its accuracy can be further enhanced if combined with accurate radiation pyrometry.

In the present phase of this study, direct observation, using high speed cinematography, of the solid-liquid interface was used because of its simplicity. The data reported here are from a weld (weld No. J-7 in Table 4) in which direct observation was facilitated because of its relatively large pitch.

Two types of measurements were made, namely growth was measured perpendicularly to the travel direction of the arc and along the weld axis. The results are summarized in Table 6 and in Figure 9. They represent growth during low pulse time. Observation of growth or melting phenomena during the high current arc presents additional experimental difficulties and has not been attempted during this phase of the study. The succession of events during a low pulse time of weld No. J-7 (t_p = 0.208 s, t_b = 0.832 s) is as follows:

After the end of high pulse current for about 50 to 80 ms, melting continued in both the forward and transverse directions to the weld axis, except in the tail part of the pool. In Table 6 melting is

indicated by the negative sign of the growth rate. Positive growth was initiated after this period.

The growth rate, in general, varied between approximately 1 mm/s and 8 mm/s. The maximum growth rates appeared between 120 and 200 ms after the end of the high pulse current, but later the rate generally diminished to somewhere between 1 and 2 mm/s. Finally in the last 150 ms of the low pulse time, the growth rate increased again; gradually in the beginning but very rapidly towards the end.

Assuming that the temperature gradient in the liquid side of the solid-liquid interface was at least as large as the minimum measured on the solid side (actually it is expected to be much larger because of the substantial drop of temperature - 70°K - measured at the interface, see Table 5) and on the basis of the growth rate reported here, the G/R ratio can be estimated. Thus for a G_L = 1030°K/mm and a growth rate varying between 1.0 and 8.0 mm/sec., the limits for G/R can be estimated as follows for the welds under consideration.

$$1.33 \times 10^4 \ \ ^\circ K \cdot s \cdot cm^{-2} < G/R < 1.07 \times 10^5 \ \ ^\circ K \cdot s \cdot cm^{-2}$$

The lower limit in this relationship is near the value reported by G. R. Purdy[60] (10^4 °C·s·cm^{-2}) as necessary for the transition to cellular growth for Fe-8%Ni alloy. Indeed the structure of these welds was found to be almost 100% cellular with very few areas in which secondary arms could be discerned and only on a limited local basis, see Figures 10 through 12.

The cellular structure of these welds, however, show an unusual variety of cell sizes. This means that the cell size changes rather abruptly for adjacent grains and in many cases within the same grain, see for example Figure 10. These variations can be explained on the basis of the observed flow patterns in the liquid pool. It appears that the arc is emitting rather frequently "tornado like" turbulence which is causing the liquid in the pool to rotate basically in two directions: (a) around the arc, and (b) around the "eye of each

"tornado". The interaction of this type of flow with the advancing solid front can easily cause the cell size to fluctuate, even within the same grain. Welds made with higher arc travel velocity show some secondary branching, i.e., dendritic growth, near the weld axis, but this may be explained as relating to the lack of intense fluid flow in the tail part of the weld pool.

4.3 Computational Estimates

Computer model predictions are, in part, based on certain material properties, i.e., C_p, k or α, and on knowing the portion of arc energy transferred to the weld plate (H_{net}). Estimates of these properties and the heat transfer efficiency (μ_I) were, therefore, necessary. The methodology for estimating these constants has been described earlier. Estimates of thermal conductivity, specific heat and thermal diffusivity are given in Figures 13, 14 and 15 respectively.

Heat transfer efficiency is the ratio of net energy input to total arc energy, as was defined in Table 2. The rate of heat input (Q, $cal.s^{-1}$) can be calculated from Wells' equation for the three arc travel speeds used in the experiments, and $T_m = 1733°K$, $\alpha = 0.0505\ cm^2.s^{-1}$, $k = 0.597\ cal.s^{-1}cm^{-1}K^{-1}$, and $\delta = 0.081$ cm. Then the following equations are obtained relating Q to bead width:

for $v = 0.2117\ cm\ s^{-1}$ $\quad Q = 70.56\ d + 13.47$

$v = 0.4233\ cm\ s^{-1}$ $\quad Q = 141.09\ d + 13.47$

$v = 0.6054\ cm\ s^{-1}$ $\quad Q = 201.78\ d + 13.47$

The three lines represented by these equations intersect at $Q = 13.47\ cal.s^{-1}$ at which no melting is expected, as seen in Figure 16.

Bead width measurements are given in Table 7. Separate measurements are listed for the front (d_f) and the back (d_b) in the table to distinguish full penetration welds where heat flow can be assumed to be two dimensional. When d_f/d_b ratio was over 0.95, the weld was considered a full penetration weld. Table 8 is a list of the

full penetration welds for which heat transfer efficiencies were determined. H_{net} values in this table were calculated from:

$$H_{net} = \frac{Q}{v} \quad cal.cm^{-1}$$

where Q for an experimental weld can be found from Figure 16 using the bead width measurements listed in Table 7. Total arc energy per unit length, H, for the pulsed current welds were calculated from the expression

$$H = \frac{1}{4.184T} (e_p i_p t_p + e_b i_b t_b) \quad cal.cm^{-1}$$

where 4.184 is a conversion factor (w.s. to cal.), and e is the arc voltage. The values of i_p, i_b, t_p, t_b and T for all of the welds can be found in Table 3 and e values corresponding to every i_p and i_b may be obtained from the voltage-current characteristic of the welding arc shown in Figure 5. The underlying assumption here is that for a square current waveform, such as that shown in Figure 3, an arc voltage waveform of square shape develops. Studies on thermal decay of arcs[61,62] show that arc voltage response to current change occurs in less than a millisecond. The error arising from this assumption should, therefore, be minimal.

The heat transfer efficiency, μ_I, for a pulsed current weld in Table 8 is an average value representing both high and the low pulse arcs. A rough estimate of the heat transfer efficiency for the high pulse current arcs may be made from the expression:

$$H_{net} = H \cdot \mu_I = 0.239 \frac{1}{T.v} (i_p e_p t_p \mu_p + i_b e_b t_b \mu_b)$$

where μ_p and μ_b are heat transfer efficiencies for the high and low pulse arcs respectively. Equations with two unknowns may be set up for the welds having the same i_p and i_b values to solve for μ_p and μ_b. When this was done μ_b values found were scattered around zero, with some positive and some negative values. By assuming $\mu_b = 0$, heat transfer

efficiencies for high pulse current arcs for a selected number of pulsed current welds representing a matrix of high/medium/low pitches and high/medium/low heat inputs were calculated and are given in Table 9. Such heat input rates were then used to calculate, through the computer model, various solidification parameters such as temperature, temperature gradients and growth rates.

The model predictions for the weld No. J-7, for example, were as follows. The temperature profile along the axis of weld J-7, a few tenths of a millisecond before the transition from i_p to i_b is shown in Figure 17. At this point in time the arc is 1.3 mm away from the most advanced point of the pool and 2.7 mm from the trailing end of it. The respective temperature gradients in the solid at the solid-liquid interface were found to be 1412°K/mm and 860°K/mm ahead and behind the arc. The temperature profiles transverse to the weld axis at the point of arc impingement after the $i_p \rightarrow i_b$ transition is shown in Figure 18. The weld pool is expected to be completely solid 600 ms after the $i_p \rightarrow i_b$ transition and the predicted maximum width of the pool is approximately 5 mm. The predicted maximum temperature gradient at the solid-liquid interface (G_s), a few tenths of a millisecond prior to the $i_p \rightarrow i_b$ transition, remains basically unchanged after the transition for at least another half a millisecond. The predicted value of G_s for this period is approximately 884°K/mm. At about 100 ms after the $i_p \rightarrow i_b$ transition, the G_s for the same site remains as high at 500°K/mm.

The predicted growth rates transverse (R_t) and along (R_w) the weld axis are shown in Table 10. They indicate a surge for growth for R_t immediately after the $i_p \rightarrow i_b$ transition, and another surge for growth, for R_w, towards the end of solidification.

4.4 Comparisons of Computational and Experimental Data

In the preceding paragraphs both experimental and computational data from a pulsed arc welding test (J-7) have been presented. These data refer basically to temperature distribution, temperature gradient G_s and growth rates for the particular weld under consideration. Comparison of the experimental and computational data for these parameters shows that:

(a) The computational temperature profiles appear to be somewhat short of the actual. Thus, whereas the measured bead width for test J-7 averages 7 mm, the maximum bead width computed is only slightly larger than 5 mm. Although the agreement is not fully satisfactory, high speed cinematography shows that a cold margin approximately 1 mm wide exists on both sides of the liquid pool for the entire t_b time period. It appears, therefore, that the experimentally measured bead width may actually be slightly smaller than what appears to be after the welding is finished. Nevertheless, additional study of the flow conditions in the pool and appropriate adjustments of the conductivity in this area are indicated if the agreement between experimental and computational data is to be improved.

(b) The computational maxima temperature gradients in the solid are within 10-15% of the experimentally determined ones (1030°K/mm vs 884°K/mm). The agreement is considered very good.

(c) The growth rate data show considerable variations between the experimental (Table 6) and the computational (Table 10) values. This must be at least partially attributed to the difficulty in estimating experimentally the exact position of the solid front as well as the lack of a more dense matrix of computational data in this phase of

the study. It must be said, however, that both sets of data agree on the basic trends and show a surge of lateral growth shortly after the $i_p \rightarrow i_b$ transition with very similar growth rates (4.32 to 5.41 vs 5.55 $mm.s^{-1}$ for this period) and a slow down after about 100 ms (1.00 to 3.60 vs 3.85 $mm.s^{-1}$). What is more important is the agreement between the computed and measured values for the G/R parameter with those required for the formation of the experimentally observed solidification structure. Here the agreement is very good.

Finally, an area of weakness is the difference that exists between the computational and the experimental data with regard to the time at which solidification is complete in the pool. This difference is of the order of 200 ms (the computational time is shorter) and it must be related with the mass transport phenomena that accompany the solidification process which are not accounted for in the computer simulation.

4.5 Melting Efficiency

Melting efficiency for all of the welds listed in Table 3 was also calculated by determining the volume of weld nugget per unit length from bead width measurements, and the heat content of the molten alloy at the melting point. The latter is the energy required to melt weld nugget of unit length, H_m, which when divided by the total arc energy, H, yields the melting efficiency of the process, μ_2.

The dotted line representing C_p in Figure 14 obeys the following equation within 100° - 1746°K where 1746°K is the liquidus temperature for Fe-26Ni obtained from the phase diagram:

$$\log C_p = 0.154 \log T - 1.327$$

or

$$\ln C_p = 0.154 \ln T - 3.055$$

$$C_p = \exp (0.154 \ln T - 3.055)$$

Assuming that the base plate was 25°C (298°K) prior to the start of welding, the change in the heat content of a 1 g mass of the weld nugget metal due to rise of its temperature to 1746°K is

$$H_{1746} - H_{298} = \int_{298}^{1746} \exp\,(0.154 \ln T - 3.055)\, dT$$

Taking $H_{298} = 0$ and integrating we find:

$$H_T = 0.04083\ T^{1.154}$$

$$H_{1746} = 225 \ \text{cal.g}^{-1}$$

The latent heat of fusion for the Fe-26Ni alloy has been estimated[56,57] to be 88.5 cal.g^{-1}, so that 313.5 cal.g^{-1} of the arc heat is used for melting one gram of the alloy. H_m values are then found from:

$$H_m = (313.5)\rho\delta\,\frac{d_f + d_b}{2} \ \text{cal.cm}^{-1}$$

Table 11 lists H, H_m and μ_2 values calculated for the welds, and Figure 19 shows the effects of total arc energy and arc travel speed on melting efficiency regardless of the specific welding variable combinations used. Two trends are obvious: melting efficiency increases with increasing H and v. The latter effect is predicted by the Wells' equation given earlier relating heat input rate to bead width.

4.6 Effects of Pulsing Parameters

For the lowest travel speed the scatter in pulsed current data in Figure 19 is probably largely a consequence of changing pulsing variables from one weld to the next. The individual effects of the pulsing variables i_p, t_p and f, and P are shown in Figures 20, 21 and 22, respectively. It is seen that increasing high pulse current, which

is accompanied by an increase in total arc energy, increases melting efficiency (Figure 20). Some increase in melting efficiency is also obtained when high pulse time is increased, or frequency is decreased, while keeping total arc energy/cm, H, constant. Large pitch values obtained solely by increasing low pulse time and/or arc travel speed, with i_p, t_p and i_b constant, has a dramatic effect on bead width without influencing melting efficiency as seen in Figure 22.

Pulsing seems to add little to the melting efficiency of the GTAW process, mainly because of the V-I characteristic of the power supply (Figure 5). Arc energy generated during the low pulse time is probably largely being wasted while adding considerably to the value of total arc energy computed, because of the high arc voltage at low currents. This can be seen by comparing welds H1 and H2 with other welds of similar total arc energy such as G3 and G8. The former two welds had higher heat transfer (Table 8) and melting (Table 11) efficiencies than G3 and G8 because of their higher low pulse currents, and hence lower corresponding arc voltages. Use of power supplies with relatively more constant potential characteristic or selection of i_b and i_p values in a way to keep arc voltage low should improve pulsed current melting efficiency. Electrode type, size and shape, arc atmosphere and arc gap are other variables which, if properly selected, may produce a more constant voltage over a wide arc current range leading to higher melting efficiencies in PC-GTAW.

5.0 SUMMARY

The first year's effort was concentrated on the development of a predictive computer model of pulsed arc welding of thin sheets under two dimensional heat flow, establishing the experimental techniques to develop physical data to correlate process variables to weld solidification structure, and comparative analysis of experimental data and model predictions for further refinement of the computer model. These tasks were successfully accomplished.

A large number of pulsed current GTA welds were made in thin sheets of Fe-26Ni binary alloy selected as the material system model. Experimental welds were dimensionally and structurally analyzed, welding process and the weld pool kinetics were studied through high speed cinematography and conventional, as well as scanning electron metallography. Temperature histories of various locations at and around weld pools developed under several sets of pulsed current welding conditions were experimentally recorded. All experimental data were evaluated and comparatively analyzed against the early predictions of the computer heat-flow model. Certain material properties and heat transfer efficiency of the pulsed current welding were estimated for use as computer input. In addition, melting efficiency of the process under various sets of pulsed welding variables was determined.

This research effort so far has established an experimental and a computational approach to study the pulsed arc welding process. The agreement between the experimental and the computational data was good with regard to temperature profiles, temperature gradients and the G/R ratio. Additional work and data are needed to further refine both the experimental and computational approach in estimating local growth rates and solidification times.

Heat transfer and melting efficiencies of the PC-GTAW process improved with increasing arc travel speed, low pulse current and with increasing total arc energy per unit length. Improvements were up to

10% in the case of heat transfer efficiency and up to 30% for the melting efficiency. These figures are expected to be different for different V-I characteristics of the power supply and different electrode size, type, shape and arc atmosphere combinations. Better improvement can be expected in thermal efficiency for the PC-GTAW when compared to steady current GTAW if the arc voltage change with change in current is small for the lower ranges of current.

BIBLIOGRAPHY

1. J. N. Lanzafame and T. Z. Kattamis, "Solidification Structure of 2014 Aluminum Alloy Welds", Welding J., 52 (5) Research Suppl., 226-s to 232-s (1973).

2. T. F. Fukui and K. Namba, "Study on Metallurgical Factors Affecting Mechanical Properties of Weld-Solidified Metal in Aluminum Alloys, Trans. Jap. Welding Soc., 4 (4) 49-62 (1973).

3. G. S. Davies and J. G. Garland, "Solidification Structures and Properties of Fusion Welds", Int. Met. Reviews, 20, 83-106 (1975).

4. W. F. Savage, E. F. Nippes and S. J. Erickson, "Solidification Mechanisms in Fusion Welds", Welding J., 55 (8) Research Suppl. 213-s to 221-s (1976).

5. W. F. Savage, C. D. Lundin and R. J. Hrubec, "Segregation and Hot Cracking in Low-Alloy Quench and Tempered Steels", Welding J., 47 (9) Research Suppl. 420-s to 425-s (1968).

6. C. F. Tseng and W. F. Savage, "The Effect of Arc Oscillation", Welding J., 50 (11) 777-786 (1971).

7. T. Wada, "Solidification Processes of Weld Metals", Trans. National Research Inst. Met. (Japan), 8 (4) 136-143 (1966).

8. R. P. Simpson, "Controlled Weld Pool Solidification Structure and Resultant Properties with Yttrium Inoculation of Ti-6Al-6V-2Sn Welds", Welding J., 56 (3) Research Suppl. 67-s to 77-s (1977).

9. D. W. Becker and C. M. Adams, Jr., "Investigation of Pulsed GTA Welding Parameters", Welding J., 57 (5) Research Suppl. 134-s to 138-s (1978).

10. A. V. Petrov and V. I. Birman, "Solidification of Weld Metal in Pulsed Arc Welding", Welding Prod. 15 (6) 1-5 (1968).

11. G. A. Slavin, et.al., "Control of the Solidification Process by Means of a Dynamic Action of the Arc", Weld. Prod. 21 (8) 2-3 (1974).

12. J. G. Garland, "Weld Pool Solidification Control", Metal Constr. and Br. Welding J., p. 121 (1974).

13. A. Tzavaras, "Measurements of Microporosity by Microradiography", Trans. AIME, 32 (5) 355-362 (1965).

14. A. Tzavaras, Solidification Under Induced Fluid Flow and Continuous Casting", paper in Continuous Casting, AIME, NY, p. 197 (1973).

15. G. A. Slavin, et.al., "The Kinetics of Pool Solidification in the Pulsed Arc Welding of Sheets", Weld. Prod., 24 (1) 3-5 (1977).

16. Ralph Barhorst, Personal Communication, Hobart Bros. Tech. Ctr., Troy, Ohio (1977).

17. Eugene Vilcas, Personal Communication, Astro-Arc Co., Sun Valley, California (1977).

18. J. C. Needham, "Pulsed Current Tungsten Arc Welding", paper in Pulsed TIG Welding Seminar Handbook, Brit. Weld. Inst., Abington, Cambridge, (1973).

19. P. Boughton, "High Precision Pulsed TIG-Welding", paper in Pulsed TIG Welding Seminar Handbook, Brit. Weld. Inst., Abington, Cambridge, (1973).

20. P. Boughton and B. O. Males, "Penetration Characteristics of Pulsed TIG-Welding", paper in Pulsed TIG Welding Seminar Handbook, Brit. Weld. Inst., Abington, Cambridge, (1973).

21. G. G. Cherngshov and V. A. Danilov, "Calculating Pulsed-Arc Welding Conditions", Auto. Weld., 26 (9), 11-14 (1973).

22. P. Boughton, "The Pulsed TIG-Welding Process: Part 2 - Potential Applications", paper in Pulsed TIG Welding Seminar Handbook, Brit. Weld. Inst., (1973).

23. A. W. Carter, "Pulsed TIG-Welding of Pipes", paper in Pulsed TIG Welding Seminar Handbook, Brit. Weld. Inst., (1973).

24. G. R. Stoeckinger, "Pulsed DC High Frequency GTA Welding of Aluminum Plate", Welding J., 52 (12) Res. Suppl. 558-s to 567-s (1973).

25. R. E. Leitner, G. H. McElhinney and E. L. Pruitt, "An Investigation of Pulsed GTA Welding Variables", Welding J., 52 (9) Res. Suppl. 405-s to 410-s (1973).

26. E. P. Vilkas, "Pulsed Current and Its Applications", Welding J., 49 (4) 255-262, (1973).

27. N. S. Barabokhin, "Pulsed-Arc Welding of Alloy AMg6 in Large Thicknesses With a Consumable Electrode", Weld. Prod., 20 (3) 30-34 (1973).

28. Welding Handbook, Vol. 1, Seventh Ed., (AWS; Miami) 34-78 (1976).

29. L. M. Lobanov, A. S. Karpenko, I. M. Chertov, and I. M. Zhdanov, "Special Features of the Technology for the Pulsed Arc Welding of D-20 Alloy, and Determination of the Residual Stresses in Joints", Auto. Weld., 28 (2) 12-15 (1975).

30. G. V. Plyatsko, M. I. Moisa and L. P. Karasev, "Residual Stresses in Thin Walled Structures Reduced by the Pulsed Melting Method", Auto. Weld., 26 (2) 61-62 (1973).

31. R. G. Dickens and B. E. Pinfold, "Investigations in Pulsed Tungsten Inert-Gas Welding", paper in Pulsed TIG Welding Seminar Handbook, Brit. Weld. Inst., (1973).

32. G. A. Slavin, et.al., "The Relationship Between Technical Strength and Solidification in the Pulsed-Arc Welding of Creep-Resisting Alloys With Non-Consumable Electrodes", Weld. Prod., 18 (6) 26-29 (1971).

33. U. I. Birman and A. V. Petrov, "Influence of the Weld Metal Solidification Pattern on Hot Cracking During Pulsed-Arc Tungsten-Electrode Welding", Weld. Prod., 18 (6) 22-25 (1971).

34. G. A. Slavin, et.al., "Analysis of Pool Solidification Rates in Pulsed Arc Welding by the Factorial Procedure", Weld. Prod., 18 (8) 12-17 (1971).

35. Yu. V. Kazakov, "Structure and Properties of Joints Made by Pulsed Arc Welding Between Components of Different Thicknesses", Auto. Weld. 22 (8) 30-32, (1969).

36. G. A. Slavin, et.al., "The Structure and Solidification Cracking Resistance of Aluminum Alloy D20 in Pulsed Arc Welding", Weld. Prod., 21 (6) 34-37 (1974).

37. N. T. Dick, "Tube Welding by the Pulsed TIG Method", Paper in Pulsed TIG Welding Seminar Handbook, Brit. Weld. Inst. (1973).

38. A. A. Erokhin, et.al., "The Forced Effect of the Pulsed Arc on Welded Metal", Auto. Weld., 29 (5) 4-6 (1976).

39. N. S. Barabokhin, et.al., "The Gas-Dynamic Pressure of an Open Arc", Weld. Prod., 23 (2) 5-8 (1976).

40. G. A. Slavin and E. A. Stolpner, "Some Characteristics of an Arc Supplied With Short Pulses of Current", Weld. Prod., 21 (2) 4-6 (1974).

41. A. V. Petrov and G. A. Slavin, "The Automatic Welding of Steel Sheet Using a Pulse-Type Arc and Argon Shielding", Weld. Prod., 9 (2) 33-38 (1962).

42. T. N. Layarajan and C. E. Jackson, "Magnetic Control of Gas-Tungsten Arc Process", Welding J., 51 (8) Res. Suppl. 377-s to 385-s (1972).

43. R. J. Perry and Z. Paley, "Effects Associated With Arc Blow", Welding J., 49 (9) Res. Suppl. 389-s to 394-s (1970).

44. G. M. Ecer, "Arc Stability in Pulsed Current Welding", Proc. of the 10th National SAMPE Technical Conf., 782-791 (1978).

45. N. M. Trofimov, "Stability of DC Arc Burning in Welding With a Non-Consumable Electrode", Weld. Prod., 20 (8) 6-11 (1973).

46. N. J. Normando, "Manual Pulsed GTA Welding", Welding J., 52 (9) 566-573 (1973).

47. M. G. Vassilaros, et.al., "Heat Flow Model of Pulsed Arc Welding", to be published.

48. C. M. Adams, Jr., "Cooling Rates and Peak Temperatures in Fusion Welding", Welding J., 37 (5) Res. Suppl. 210-s to 215-s (1958).

49. A. A. Wells, "Heat Flow in Welding", Welding J., 31 (5) Res. Suppl. 263-s to 267-s (1952).

50. J. B. Wilkinson and D. R. Milner, "Heat Transfer from Arcs", Br. Welding J., 8 (2) 115-128 (1960).

51. N. D. Malmuth, W. F. Hall, B. I. Davis and C. D. Rosen, "Transient Thermal Phenomena and Weld Geometry in GTAW", Welding J., 53 (9) Res. Suppl. 388-s to 400-s (1974).

52. H. C. Ludwig, "Current Density and Anode Spot Size in the Gas Tungsten Arc", Welding J., 47 (5) Res. Suppl. (1968).

53. R. W. Niles and C. E. Jackson, "Weld Thermal Efficiency of the GTAW Process", Welding J., 54 (1) Res. Suppl. 25-s to 32-s (1975).

54. Y. S. Touloukian, R. W. Powell, C. Y. Ho and P. G. Klemens, Thermo-Physical Properties of Matter, Volumes 1 and 4, Plenum Press, New York, (1970)

55. Properties of Some Metals and Alloys, The Int. Nickel Company, New York (1968).

56. R. A. Oriani, "Thermodynamic Activities in Iron-Nickel Alloys", Acta Met., 1 (7) 448-454 (1953).

57. G. R. Zellars, et.al., "The Activities of Iron and Nickel in Liquid Fe-Ni Alloys", Trans. AIME, 215 (4) 181-185 (1959).

58. M. C. Flemings, D. R. Poirier, R. V. Barone, and H. D. Brody, "Microsegregation in Iron-Base Alloys", J. Iron and Steel Inst., 208 (4) 371-382 (1970).

59. W. F. Savage, S. S. Strunck and Y. Ishikawa, "The Effect of Electrode Geometry in Gas Tungsten-Arc Welding", Welding J., 44 (11) Res. Suppl. 489-s to 496-s (1965).

60. G. R. Purdy, Report to AISI, McMaster University (April 1970).

61. C. W. Kimblin and J. J. Lowke, "Decay and Thermal Reignition of Low Current Cylindrical Arcs", J. Applied Phys., 44 (10) 4545-4547 (1973).

62. J. J. Lowke, R. E. Voshall, and H. C. Lugwid, "Decay of Electrical Conductance and Temperature of Arc Plasmas", J. Applied Phys., 44 (8) 3513-3523 (1973).

Dwg. 6445A21

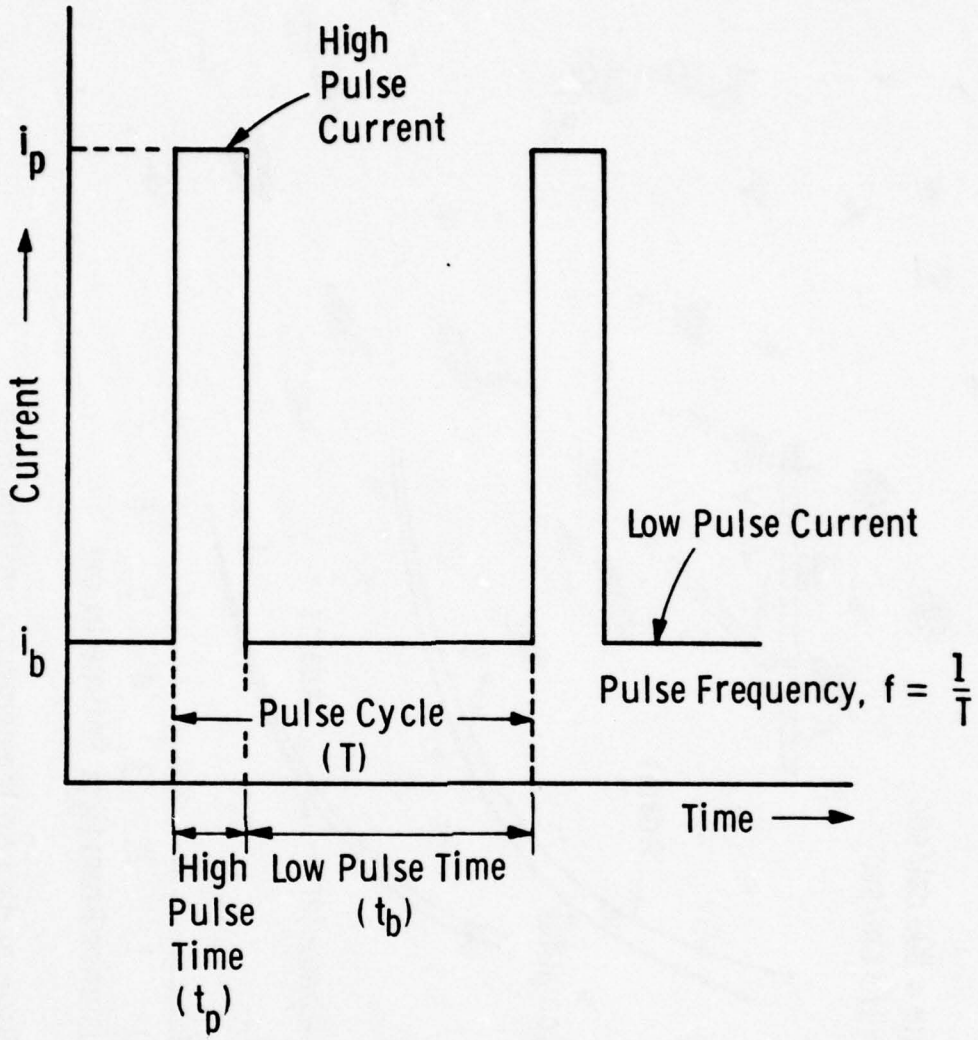

Fig. 1—An idealized pulsed current waveform and associated definitions

Curve 713476-A

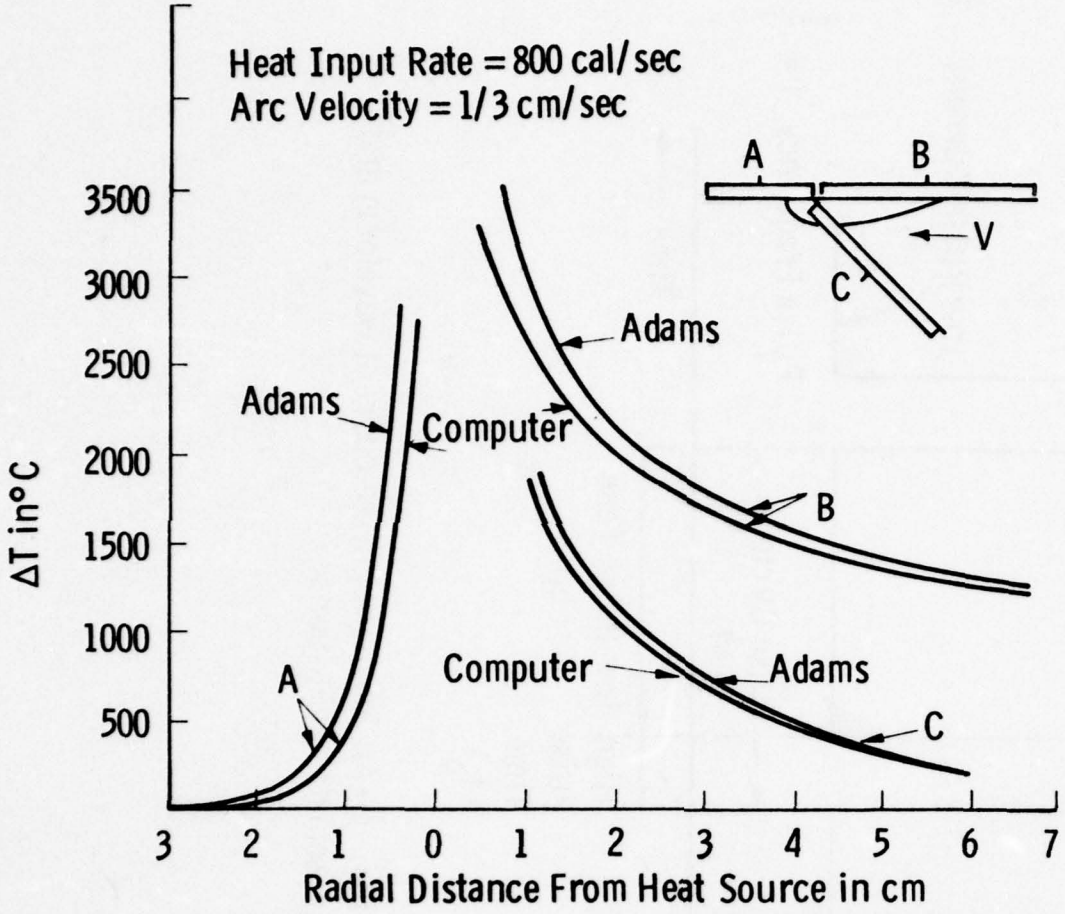

Fig. 2 — Comparison of data on temperature profiles from Adams equation and the new model for continuous arc

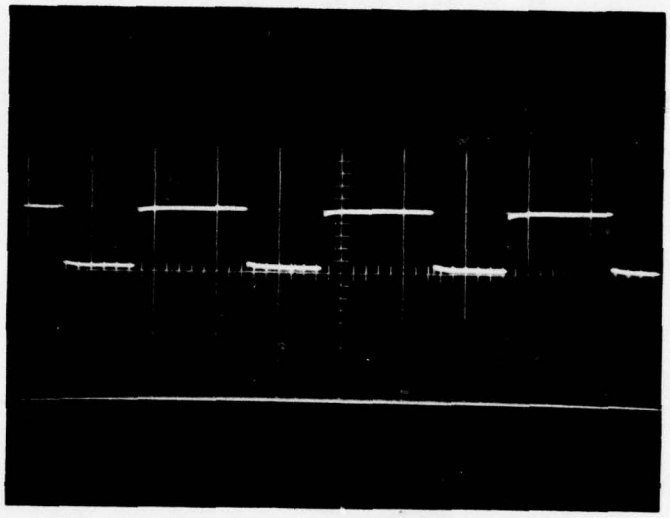

Figure 3 - A pulsed current waveform typical of those utilized in this study. Here the pulsing parameters were:

i_p = 150A

i_b = 25A

t_p = 0.009s

t_b = 0.006s

Dwg. 6445A22

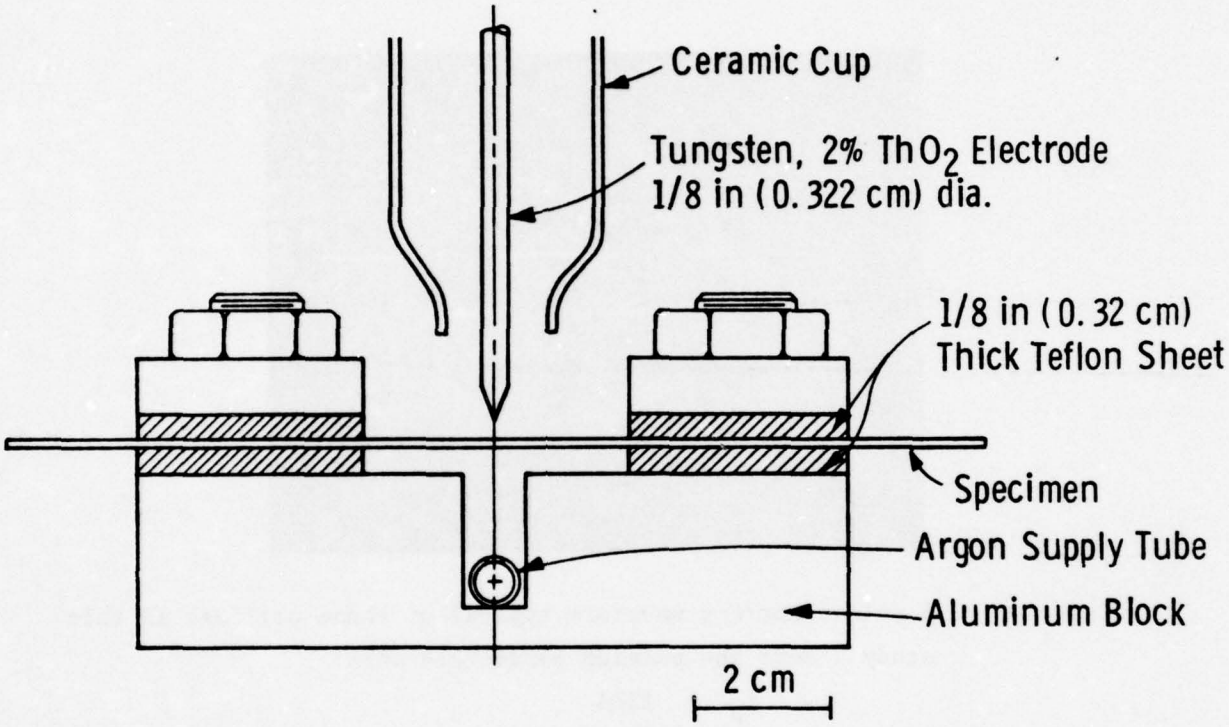

Fig. 4 —Cross-sectional view of the clamping fixture. Torch travel direction was normal to the paper

Curve 697208-A

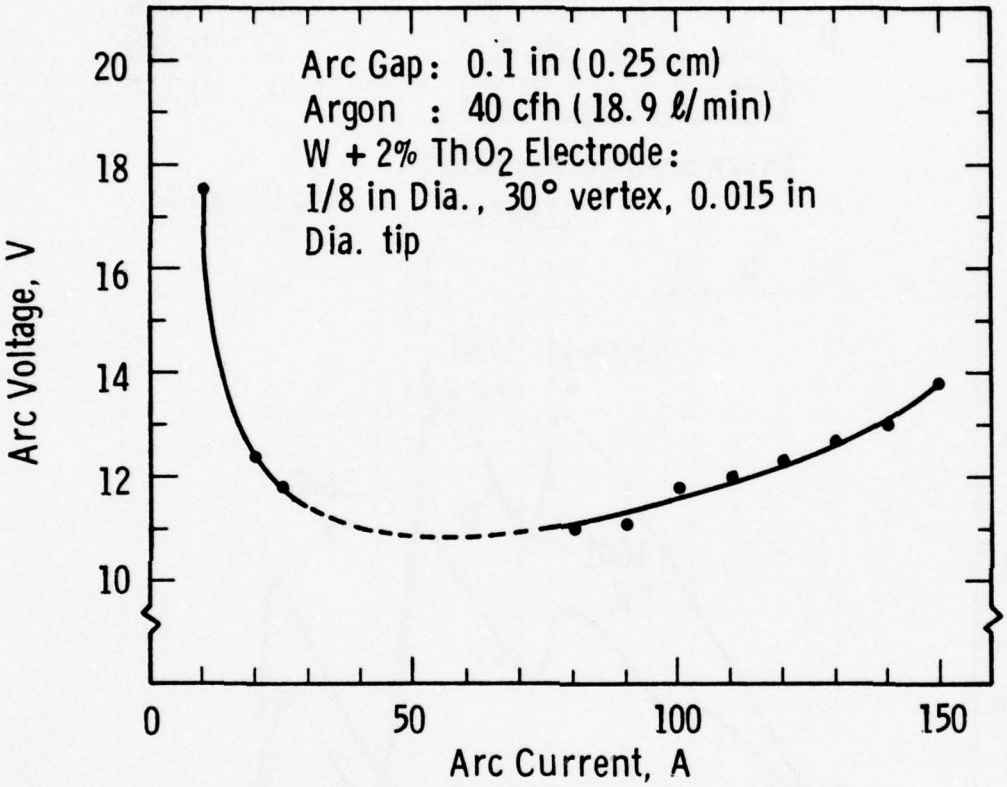

Fig. 5 —Arc voltage-current characteristic

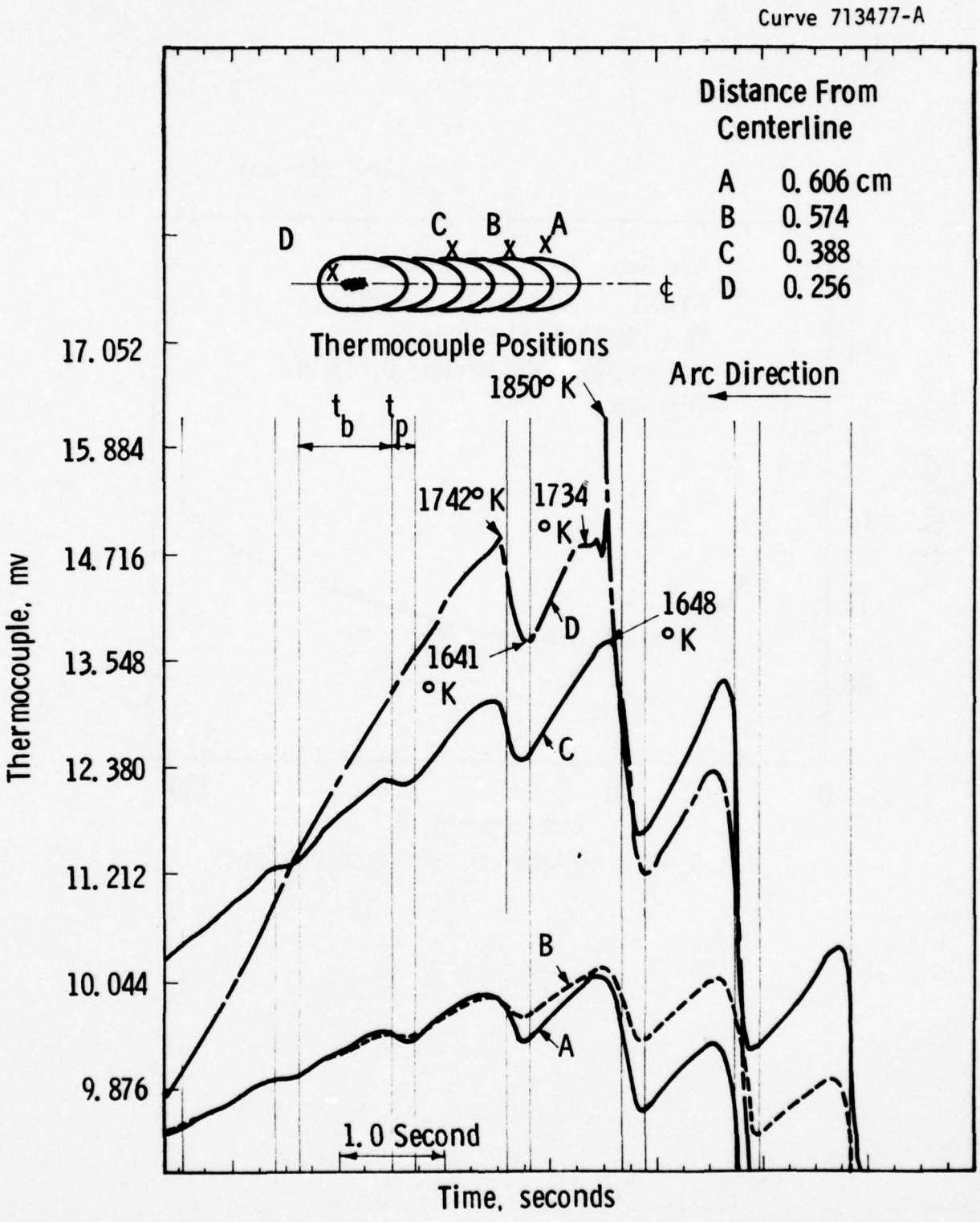

Fig. 6 — Time-temperature profiles at four thermocouple locations during welding of sample J7

Curve 712981-A

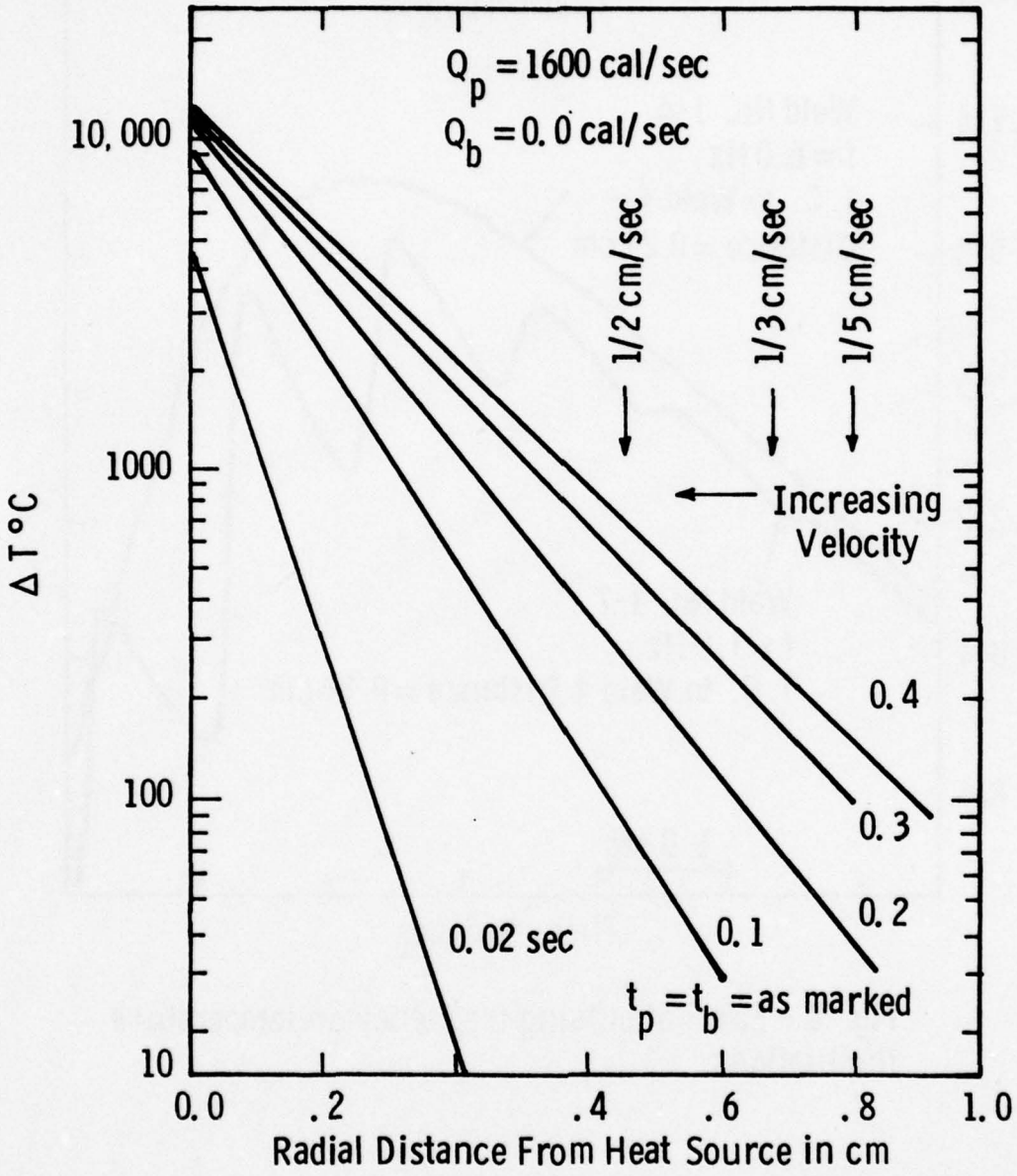

Fig. 7 – Effect of pulsing times and velocity on temperature fluctuation, ΔT, as computed from the model

Curve 712982-A

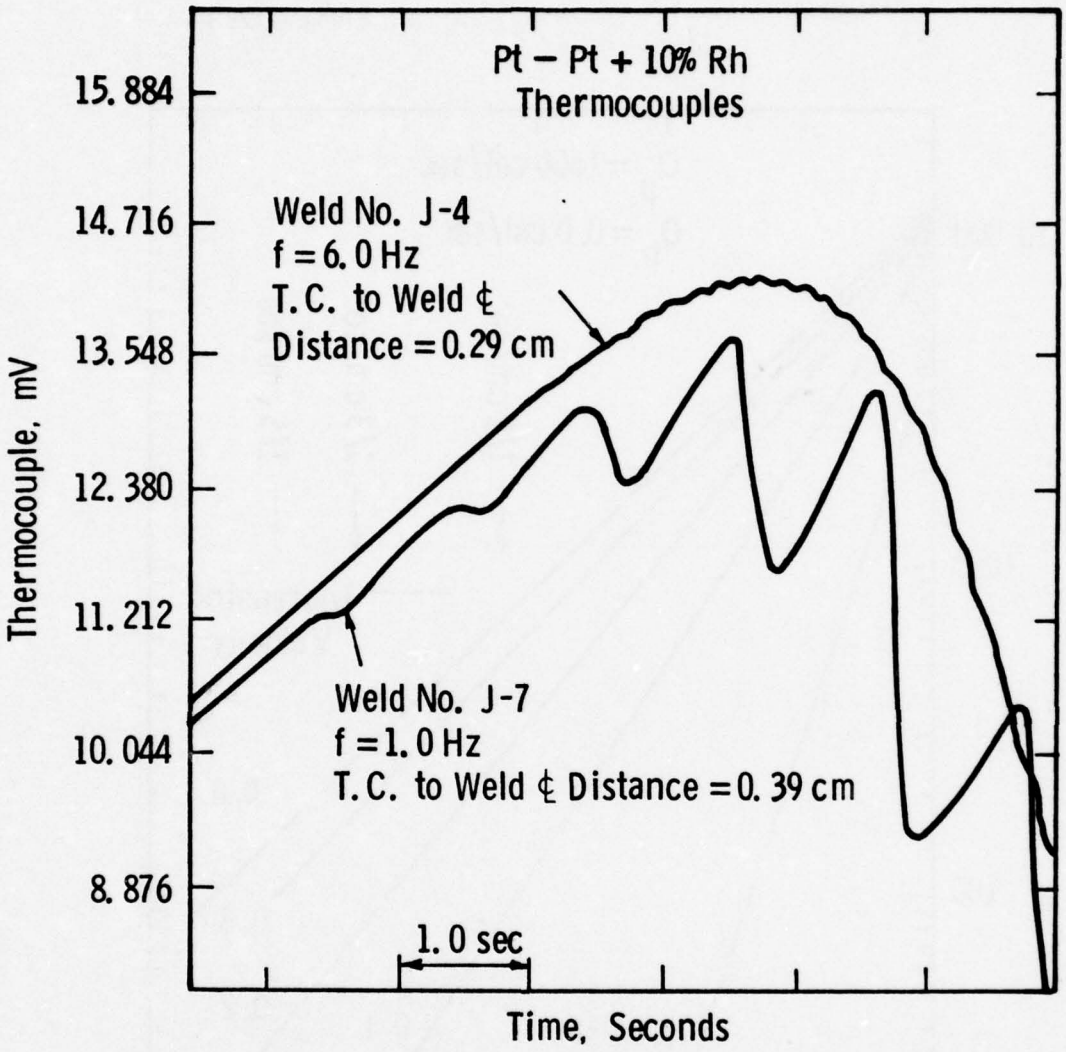

Fig. 8 – Effect of pulsing frequency on temperature fluctuations

Curve 712983-A

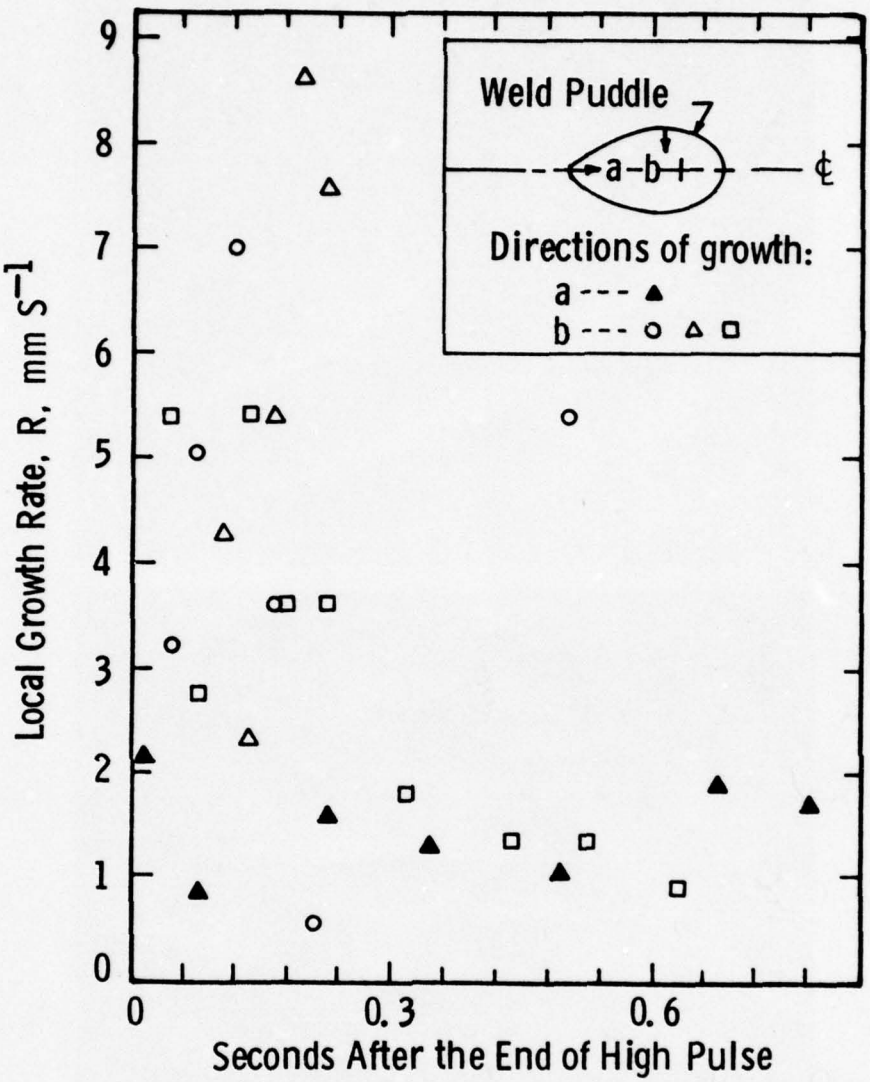

Fig. 9 — Local rates of solid growth during low pulse time for the weld No. J-7

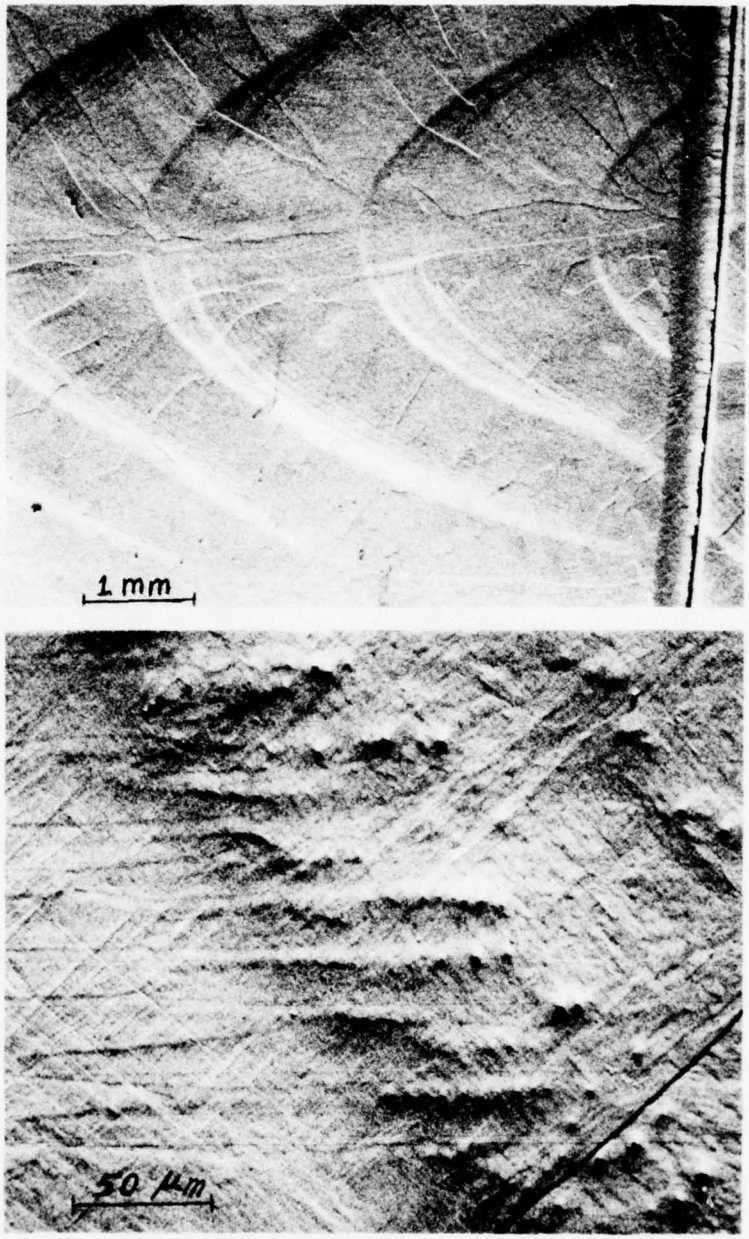

Figure 10 - Scanning electron micrographs of the weld No. J-7 showing ripple formations and solid state transformation boundaries at low magnification (top), and cells (bottom). Note varying cell size within the same grain seen at left.

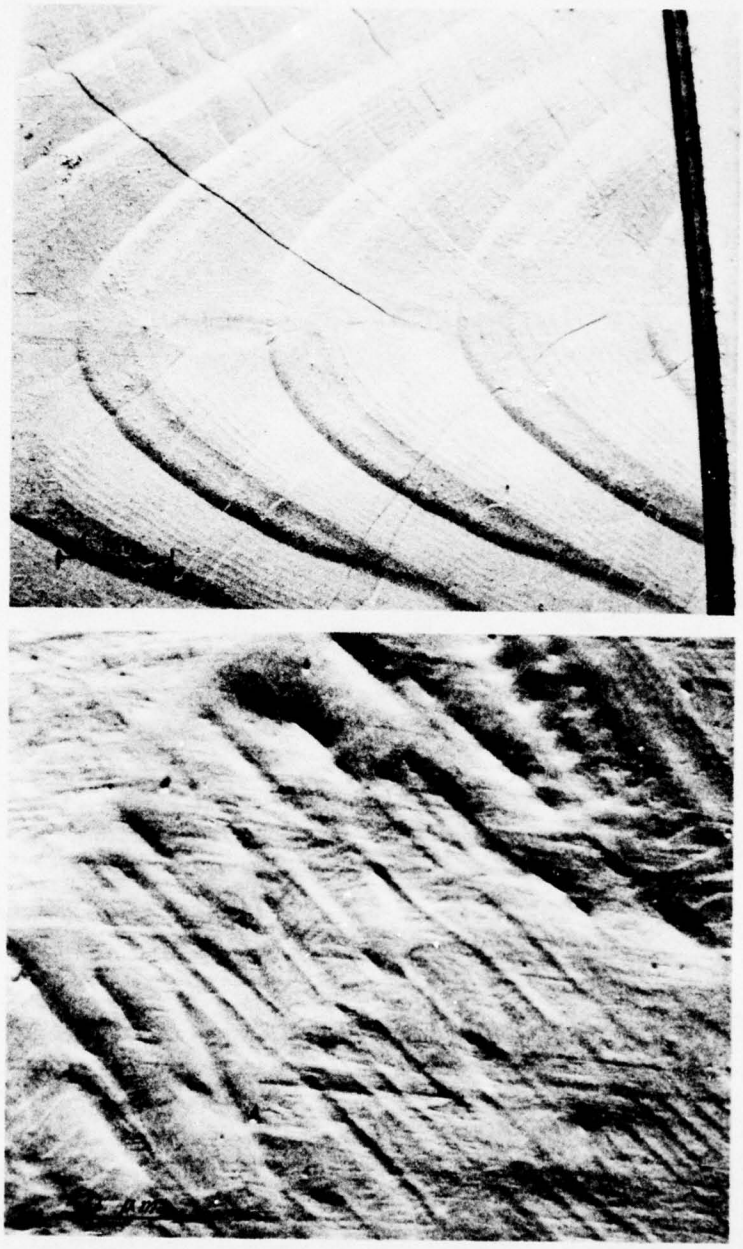

Figure 11 - Scanning electron micrographs of the weld No. G-5 showing ripple formations and solid state transformation boundaries (top), and cells (bottom).

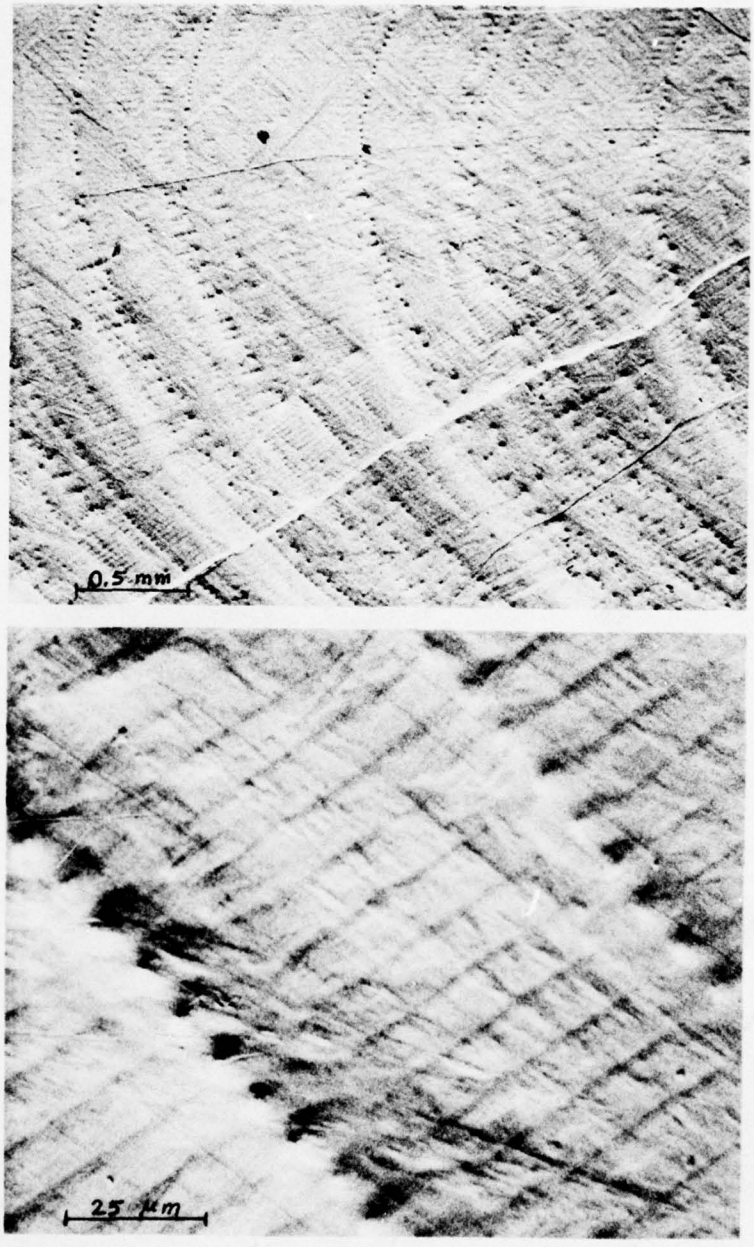

Figure 12 - Scanning electron micrographs of the weld No. F-3 showing ripple formations and solid state transformation boundaries (top), and cells (bottom).

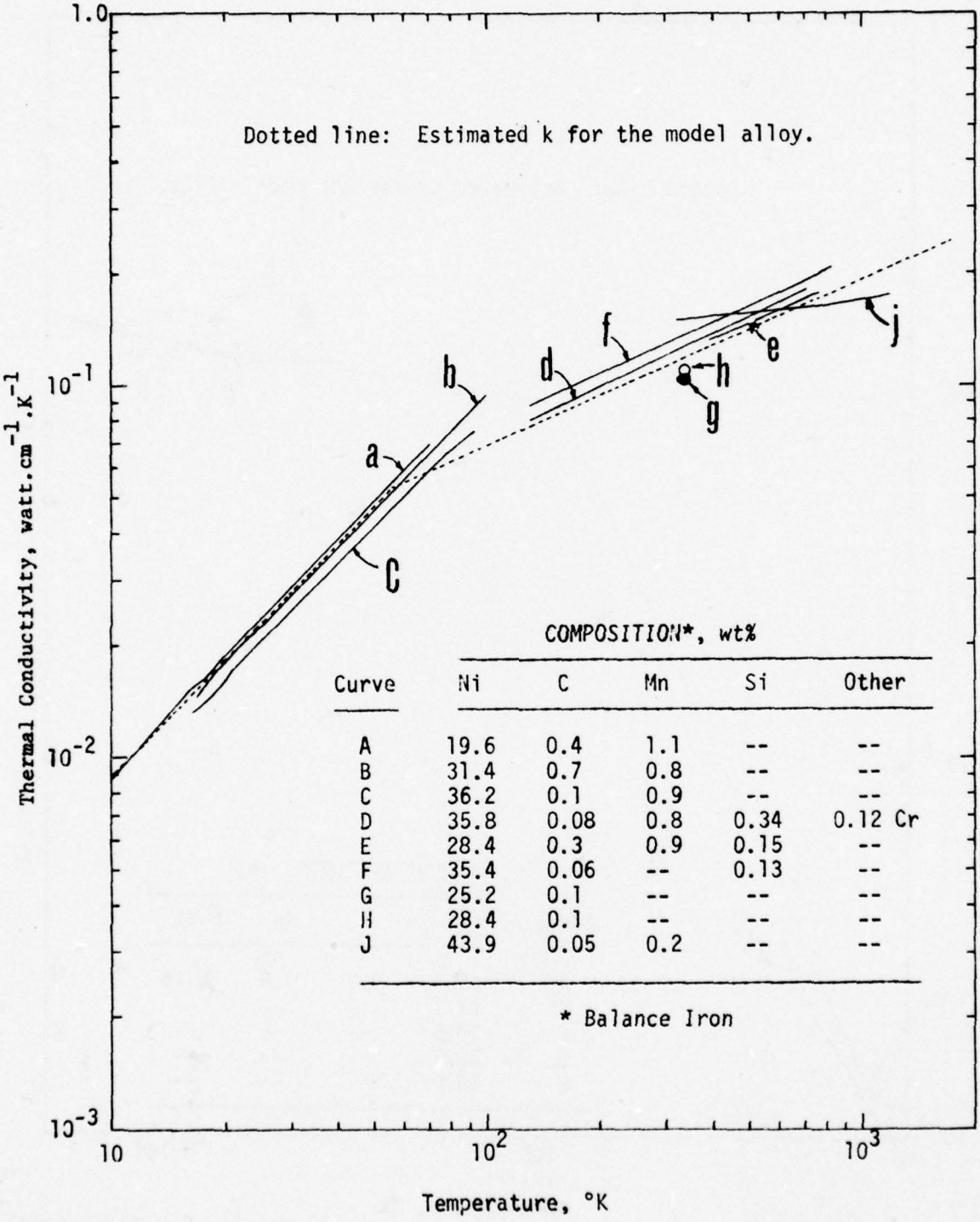

Curve	COMPOSITION*, wt% Ni	C	Mn	Si	Other
A	19.6	0.4	1.1	--	--
B	31.4	0.7	0.8	--	--
C	36.2	0.1	0.9	--	--
D	35.8	0.08	0.8	0.34	0.12 Cr
E	28.4	0.3	0.9	0.15	--
F	35.4	0.06	--	0.13	--
G	25.2	0.1	--	--	--
H	28.4	0.1	--	--	--
J	43.9	0.05	0.2	--	--

* Balance Iron

Figure 13 - Estimated thermal conductivity, k, of Fe-26Ni model alloy.

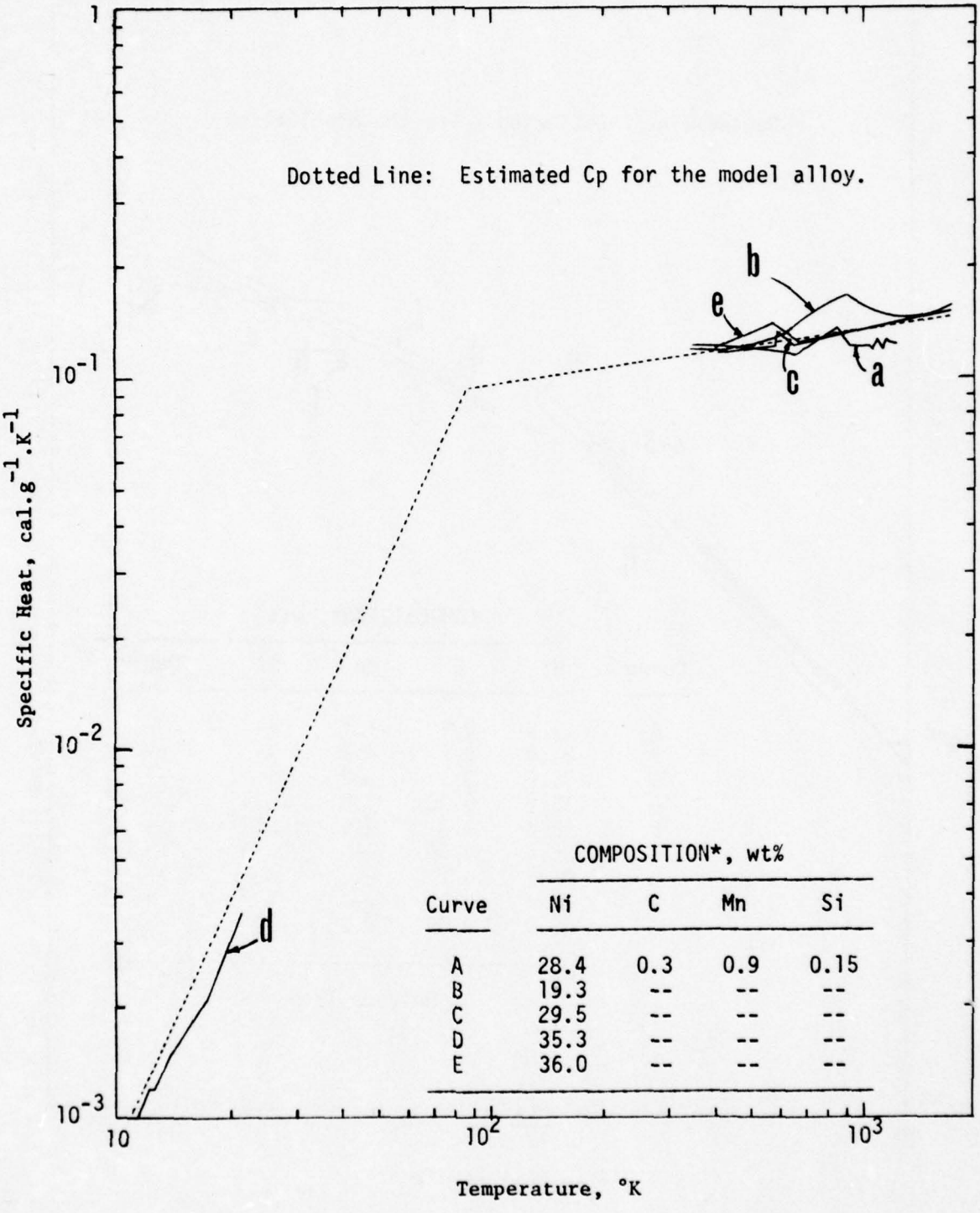

Figure 14 - Estimation of specific heat, C_p, for Fe-26Ni alloy.

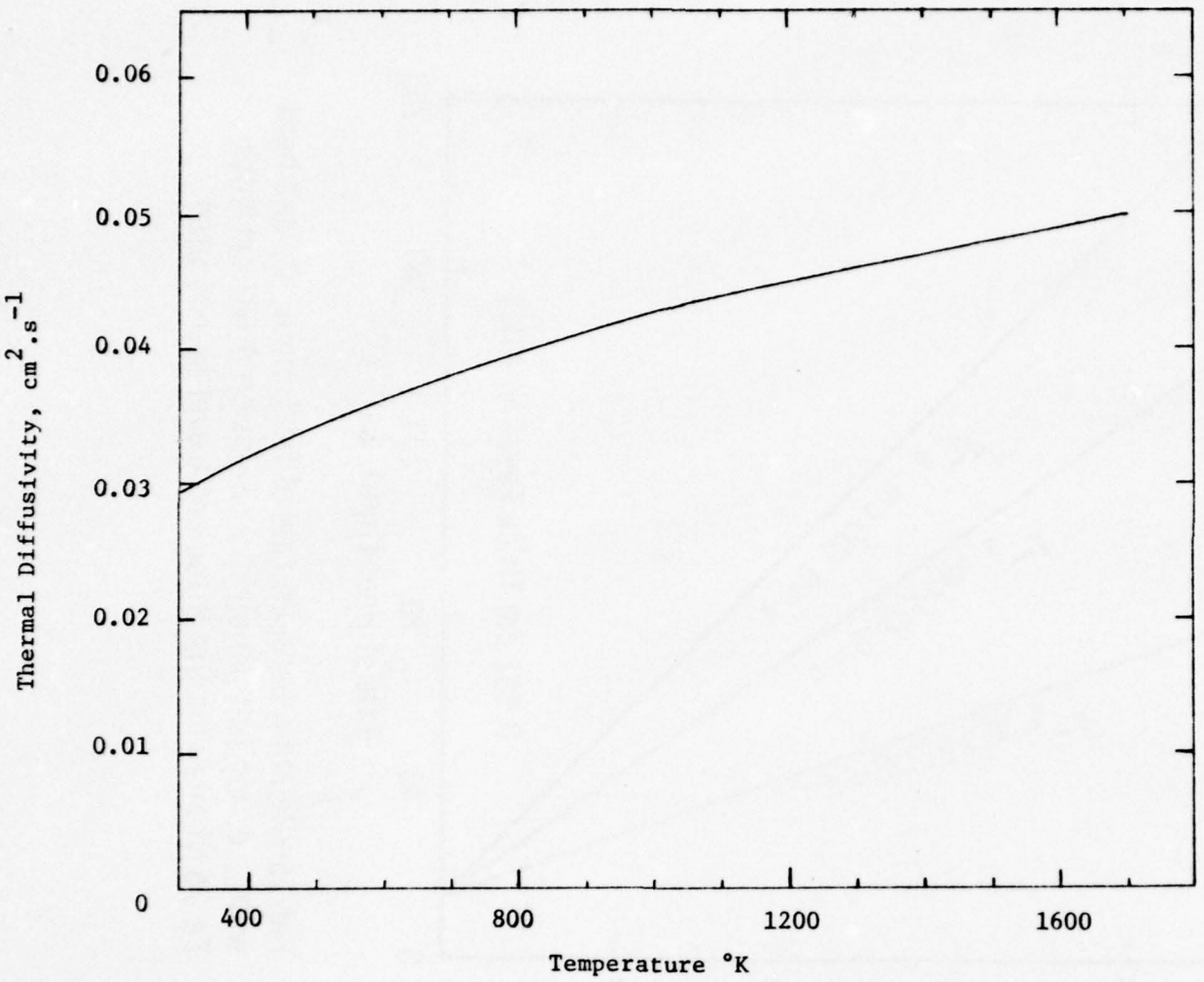

Figure 15 - Estimated Thermal Diffusivity of Fe-26 Ni Alloy.

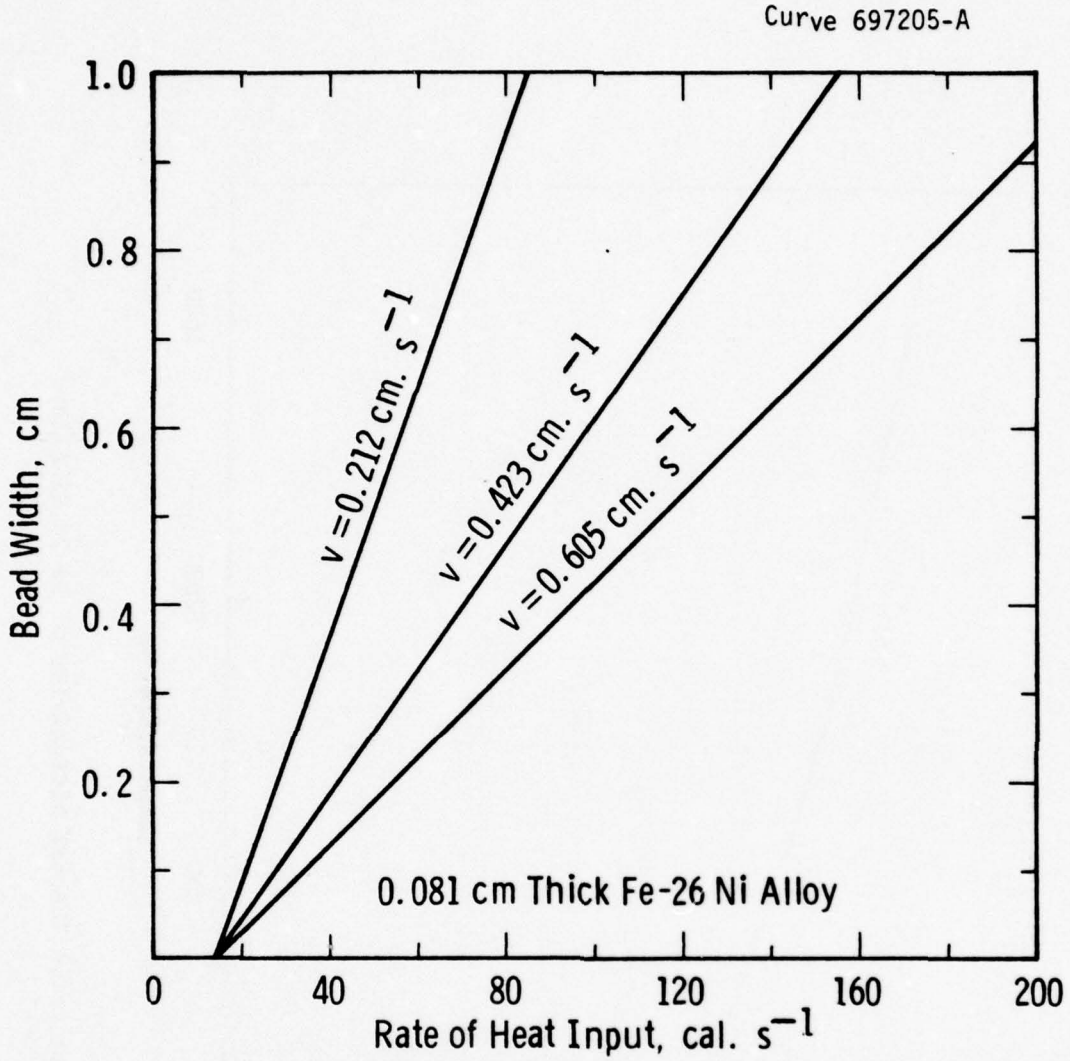

Fig. 16—Relation between rate of heat input, Q, and bead width, d, for full penetration welds on 0.081 cm thick Fe-26 Ni alloy for the three arc travel speeds used

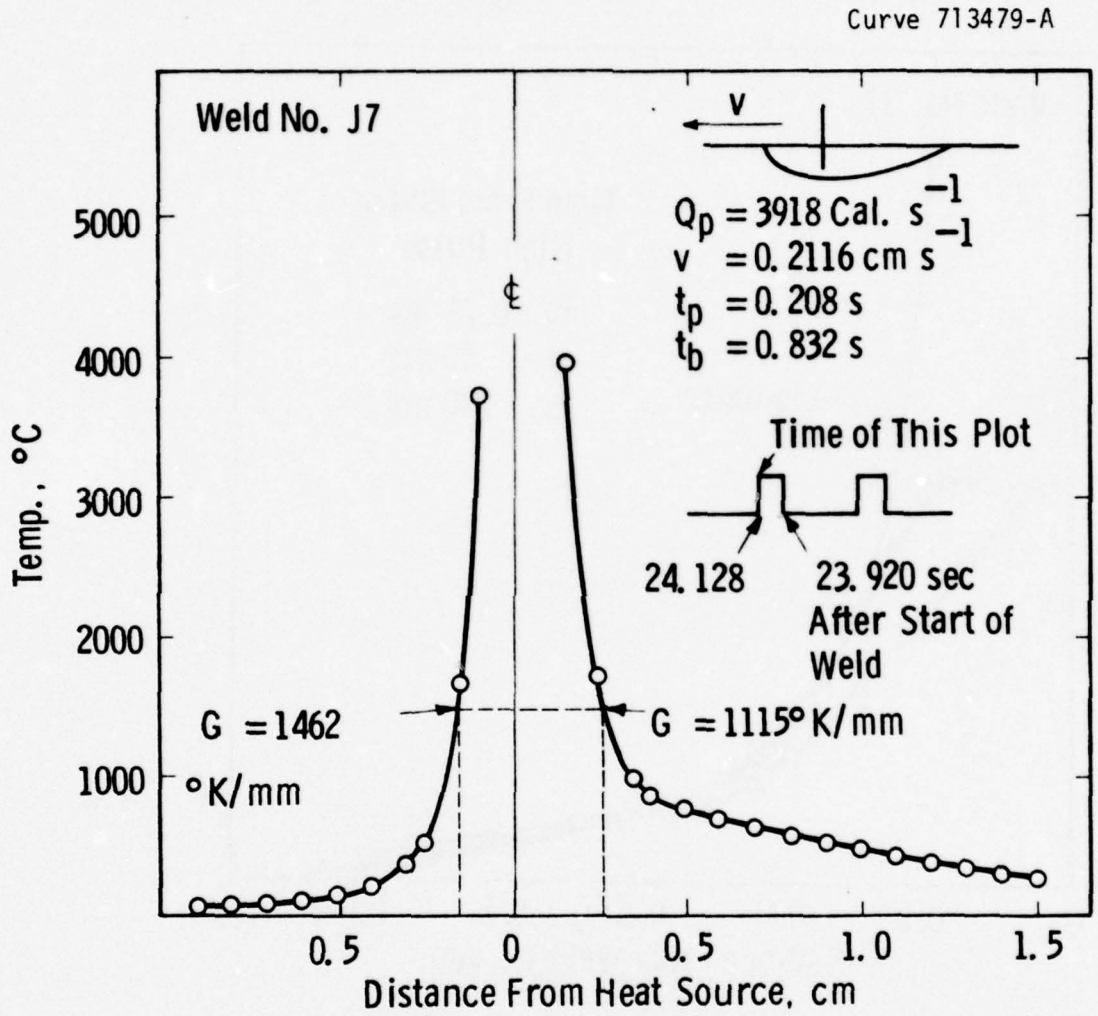

Fig. 17 — Temperature profile along the weld axis just before the end of high pulse current (computed)

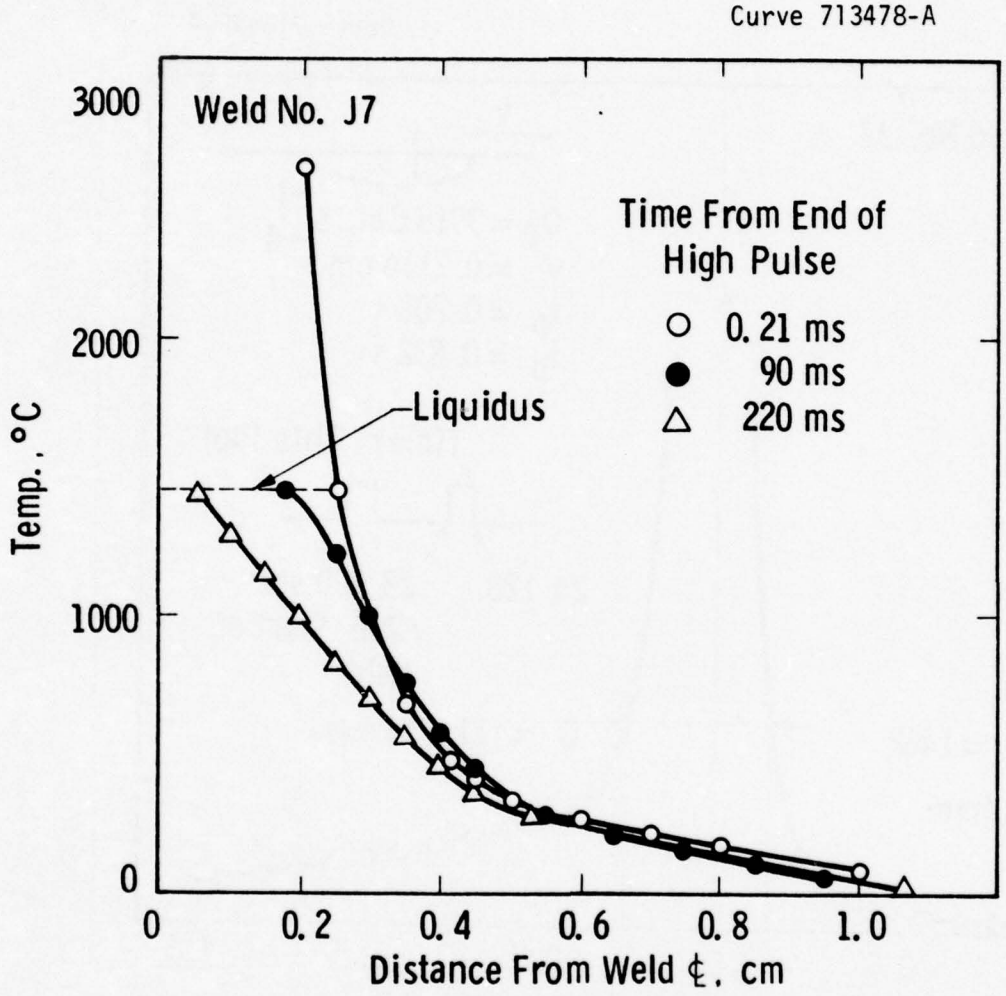

Fig. 18 — Temperature profiles along a line normal to the weld axis at the point of arc impingement at three different times from the end of high pulse current (computed)

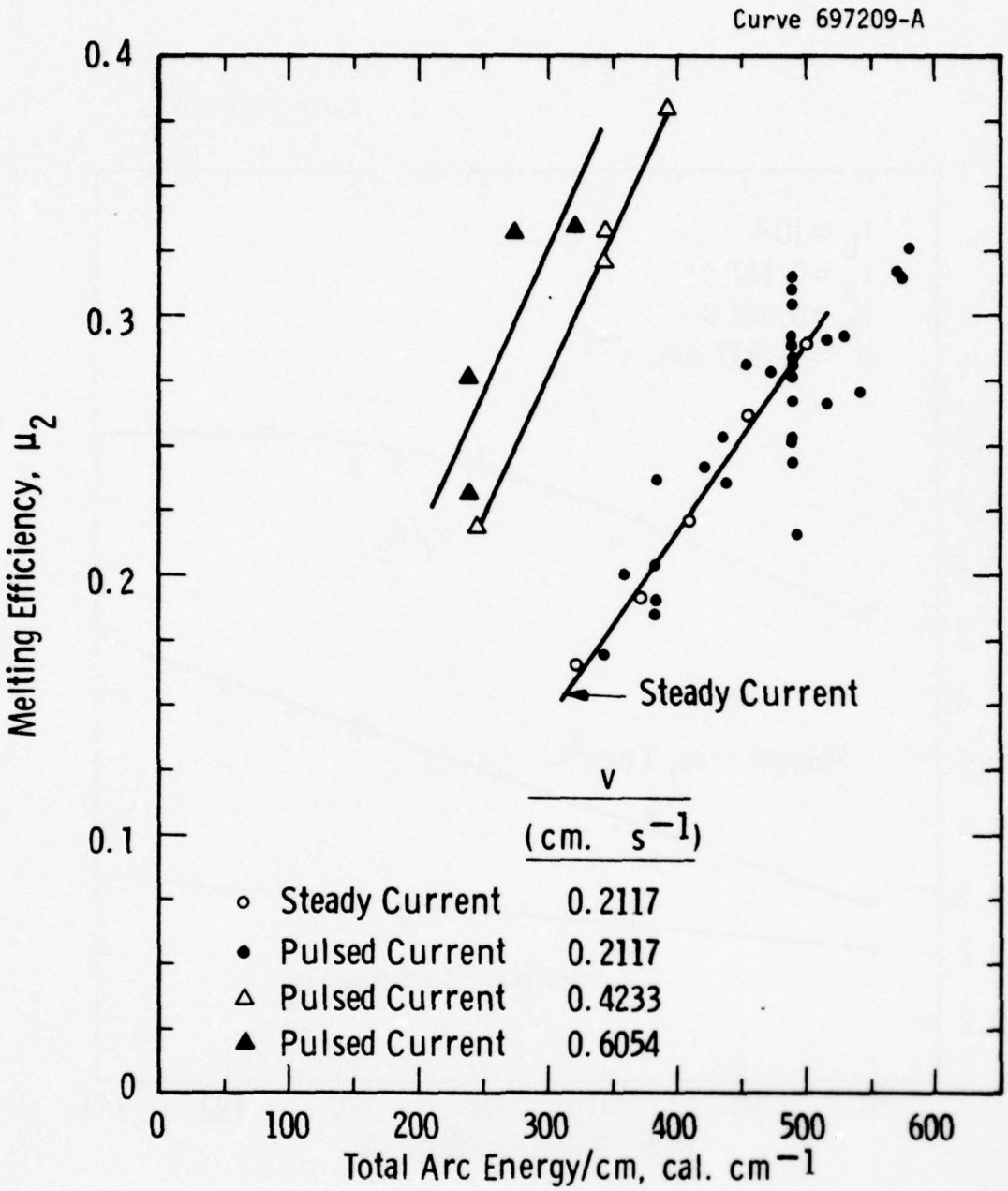

Fig. 19—Effects of total arc energy per unit length, H, and arc travel speed on melting efficiency

Curve 697207-A

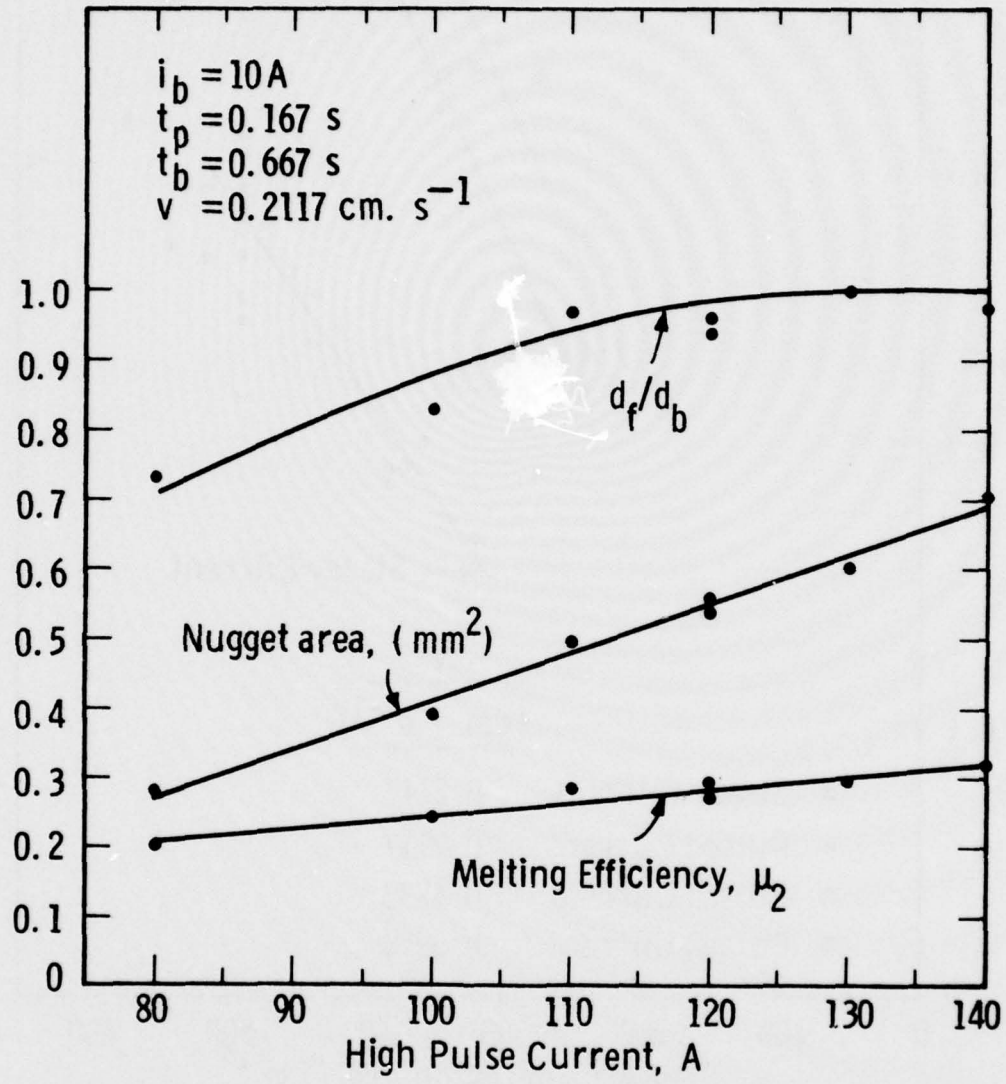

Fig. 20 —Effects of high pulse current for constant i_b, t_p, and t_b

Curve 697206-A

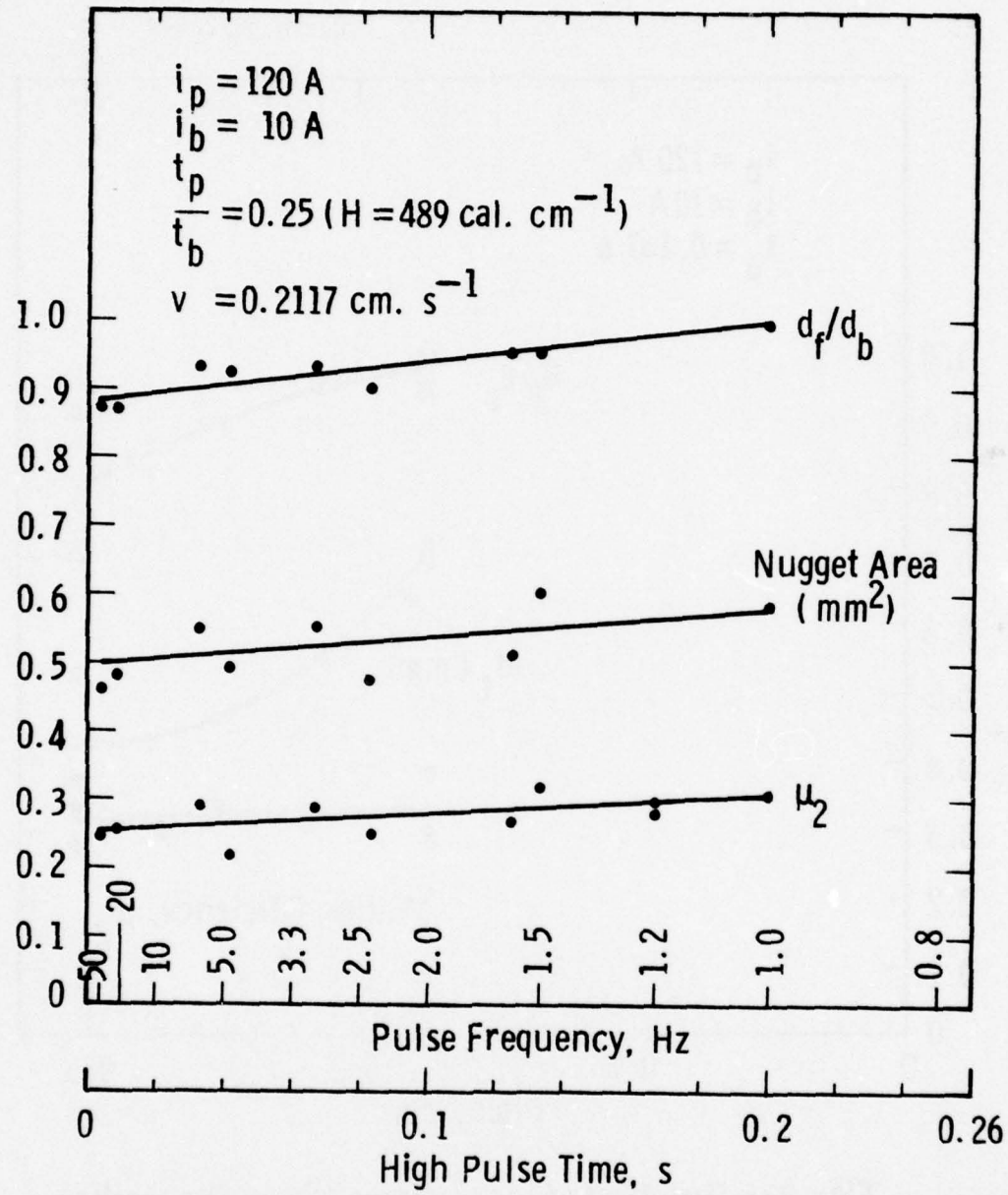

Fig. 21 — Effects of t_p, or pulse frequency, on melting efficiency, nugget area and the ratio of front and back bead widths

Curve 697204-A

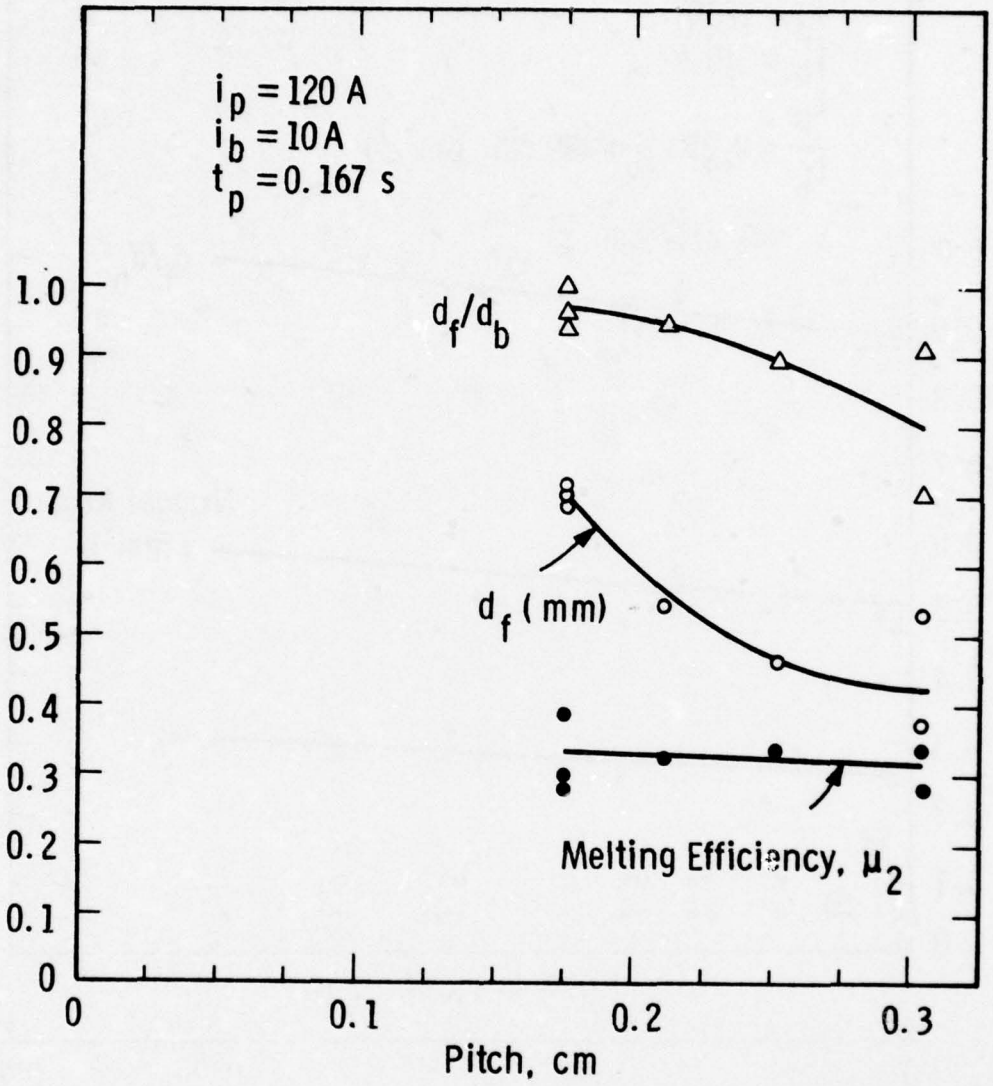

Fig. 22—The effect of increasing pitch on the melting efficiency, bead width and d_f/d_b ratio

TABLE 1

COMPARISON OF THE MAXIMUM BEAD WIDTH DIMENSIONS FOR CONTINUOUS ARCS PREDICTED BY THE WELLS' EQUATION[49] WITH THOSE BY THE PRESENT COMPUTER MODEL

q ($cal.s^{-1}.cm^{-1}$)	v ($cm.s^{-1}$)	Predicted d/2 (cm)	
		Computer	Wells'
200	0.222	0.1<d/2<0.2	0.138
1000	1.00	0.30	0.310
300	0.222	0.33	0.300
533	0.333	0.41	0.445
800	0.417	0.574	0.582
1000	0.500	0.60	0.620
800	0.333	0.775	0.720
800	0.278	0.80	0.873
1200	0.333	1.110	1.150

TABLE 2

SYMBOLS, DEFINITIONS AND UNITS OF PROCESS PARAMETERS STUDIED

Parameter	Symbol	Definition	Units
High Pulse Current	i_p	See Figure 1	A
Low Pulse Current	i_b	See Figure 1	A
High Pulse Time	t_p	See Figure 1	s
Low Pulse Time	t_b	See Figure 1	s
Pulse Frequency	f	$1/(t_p + t_b)$	Hz
Pulse Period	T	$t_p + t_b$	s
Arc Travel Speed	v	--	$cm.s^{-1}$
Pitch	P	$v(t_p + t_b)$	cm
Sheet Thickness	δ	--	cm
Weld Bead Width	d	--	cm
Arc Current	i	--	A
Arc Voltage	e	--	V
Total Arc Energy per Unit Length	H	$\frac{i \cdot e}{v}$	$\frac{1}{4.184}$ $cal.cm^{-1}$
Net Energy Input per Unit Length	H_{net}	$\mu_1 \cdot H$	$cal.cm^{-1}$
Heat Transfer Efficiency	μ_1	H_{net}/H	%
Melting Efficiency	μ_2	H_m/H	%
Energy Required to Melt Weld Nugget of Unit Length	H_m	$\mu_2 \cdot H$	$cal.cm^{-1}$
Rate of Heat Input per Unit Sheet Thickness	q	$\frac{v \cdot H_{net}}{\delta}$	$cal.s^{-1}.cm^{-1}$
Rate of Heat Input	Q	$q \cdot \delta$	$cal.s^{-1}$
Melting Point	T_m	Solidus	K
Thermal Conductivity	k	--	$cal.s^{-1}.cm^{-1}.K^{-1}$
Density	ρ	--	$g.cm^{-3}$
Specific Heat	C_p	--	$cal.g^{-1}.K^{-1}$
Thermal Diffusivity	α	$\frac{k}{C_p \cdot \rho}$	$cm^2.s^{-1}$

TABLE 3

PULSED CURRENT GTA WELDING PARAMETERS

Weld No.	i_p (A)	i_b (A)	t_p (s)	t_b (s)	v ($cm.s^{-1}$)	t_p/t_b	f (Hz)	Comments
F1	100	10	0.017	0.167	0.2117	0.10	5.4	Incomplete penetr.
F2	100	10	0.100	0.167	0.2117	0.60	3.7	Burn-through
F3	100	10	0.067	0.167	0.2117	0.40	4.3	
F4	100	10	0.033	0.167	0.2117	0.20	5.0	
F5	100	10	0.167	0.333	0.2117	0.50	2.0	
F6	100	10	0.133	0.333	0.2117	0.40	2.1	
F7	100	10	0.067	0.333	0.2117	0.20	2.5	
F8	100	10	0.090	0.333	0.2117	0.15	2.6	
G1	80	10	0.167	0.667	0.2117	0.25	1.2	
G2	100	10	0.167	0.667	0.2117	0.25	1.2	
G3	120	10	0.167	0.667	0.2117	0.25	1.2	
G4	120	10	0.167	0.667	0.2117	0.25	1.2	
G5	140	10	0.167	0.667	0.2117	0.25	1.2	
G6	150	10	0.167	0.667	0.2117	0.25	1.2	Burn-through
G7	110	10	0.167	0.667	0.2117	0.25	1.2	
G8	130	10	0.167	0.667	0.2117	0.25	1.2	
H1	100	20	0.167	0.667	0.2117	0.25	1.2	
H2	100	25	0.167	0.667	0.2117	0.25	1.2	
H3	100	5	0.167	0.667	0.2117	0.25	1.2	
H4		I=24A	Steady Current		0.2117	--	--	
H5		I=28A	Steady Current		0.2117	--	--	
H6		I=32A	Steady Current		0.2117	--	--	
H7		I=36A	Steady Current		0.2117	--	--	
H8		I=40A	Steady Current		0.2117	--	--	
J1	120	10	0.004	0.017	0.2117	0.25	47.8	
J2	120	10	0.008	0.033	0.2117	0.25	24.3	
J3	120	10	0.017	0.067	0.2117	0.25	12.0	Burn-through
J4	120	10	0.033	0.133	0.2117	0.25	6.0	
J5	120	10	0.067	0.267	0.2117	0.25	3.0	
J6	120	10	0.133	0.533	0.2117	0.25	1.5	
J7	120	10	0.208	0.832	0.2117	0.25	1.0	
J8	150	10	0.083	0.565	0.2117	0.15	1.5	
J9	150	10	0.042	0.167	0.2117	0.25	4.8	Burn-through
J10	150	10	0.033	0.250	0.2117	0.13	3.5	Burn-through
J11	150	10	0.025	0.250	0.2117	0.10	3.6	Burn-through

TABLE 3 (cont.)

Weld No.	i_p (A)	i_b (A)	t_p (s)	t_b (s)	v ($cm.s^{-1}$)	t_p/t_b	f (Hz)	Comments
K1	120	10	0.042	0.286	0.2117	0.15	3.0	
K2	120	10	0.042	0.212	0.2117	0.20	3.9	
K3	120	10	0.042	0.167	0.2117	0.25	4.8	
K4	120	10	0.042	0.135	0.2117	0.31	5.6	Burn-through
K5	120	10	0.083	0.572	0.2117	0.15	1.5	
K6	120	10	0.083	0.426	0.2117	0.20	2.0	
K7	120	10	0.083	0.333	0.2117	0.25	2.4	
K8	120	10	0.125	0.500	0.2117	0.25	1.6	
K9	120	10	0.167	0.667	0.4233	0.25	1.2	
K10	120	10	0.167	0.333	0.4233	0.50	2.0	
L1	120	10	0.167	0.250	0.4233	0.67	2.4	
L2	120	10	0.083	0.125	0.4233	0.66	4.8	Burn-through
L3	120	10	0.083	0.333	0.4233	0.25	2.4	
L4	120	10	0.083	0.167	0.4233	0.50	4.0	
L5	120	10	0.083	0.167	0.6054	0.50	4.0	
L6	120	10	0.167	0.333	0.6054	0.50	2.0	
L7	120	10	0.167	0.250	0.6054	0.67	2.4	
L8	150	10	0.167	0.333	0.6054	0.50	2.0	

TABLE 4

CHEMICAL ANALYSIS OF THE BASE METAL
USED IN THIS INVESTIGATION, IN WT%

Ni	Mn	Si	C	Fe
25.9	0.34	0.24	0.012	Balance

TABLE 5

EXPERIMENTALLY MEASURED TEMPERATURE GRADIENTS

Weld No. And Test		G_s ($°K.mm^{-1}$)	G_L ($°K.mm^{-1}$)	Distance From Fusion Line, (mm)
J-7	1	1030		0.43
	1	290		1.60
	1		131	0.89
	2	272		2.14
	2	217		2.49
J-4	1	75		2.93
	1	128		1.95
	1		25	1.10
	1*		0	0

*Temperature difference 70°K was recorded over the solidus temperature of the alloy at a site on the weld fusion line.

TABLE 6

RATE OF SOLID-LIQUID INTERFACE MOVEMENT IN WELD NO. J-7,
AS DETERMINED FROM HIGH SPEED MOVIES

Successive Low Pulse Times	Time Elapsed After $i_p \rightarrow i_b$ (ms)	Interface Speed, ($mm.s^{-1}$)	Remarks
1	0		ARC-OFF
	15.6	-2.16	Negative growth
	78.1	-2.16	the solid receeds.
	109.4	+4.32	Growth measured
	140.6	+2.32	across the bead
	171.8	+5.40	axis.
	203.1	+8.64	
	234.4	+7.56	
2	0		ARC-OFF
	15.6	-5.41	Negative growth
	31.2	+5.41	Growth measured
	62.5	+2.71	across the bead
	93.7	-	axis.
	125.0	+5.41	
	171.9	+3.60	
	281.7	+3.60	
	312.5	+1.80	
	437.5	+1.35	
	531.2	+1.35	
	640.6	+0.93	
	796.7	+9.07	
3	0		ARC-OFF
	15.6	-10.8	Negative growth
	31.2	-10.8	
	46.8	-10.8	
	77.7	+ 3.23	
	115.0	+ 5.05	
	172.0	+ 7.02	
	187.4	+ 3.60	
	515.6	+ 0.57	
	548.0	+ 5.41	
4	0		ARC-OFF
	15.6	+ 2.16	
	62.5	+ 0.86	Growth parallel to
	218.7	+ 1.63	the bead axis, at
	343.7	+ 1.30	the axis. No
	500.0	+ 1.08	negative growth
	687.5	+ 1.86	observed
	796.8	+ 1.73	
	843.7		

TABLE 7

BEAD WIDTH MEASUREMENTS

Weld No.	Bead Width (cm) Front, d_f	Back, d_b	Ratio d_b/d_f	Nugget Area (cm^2)
F1	0.27	0	Incomplete penetration	
F2	--	--	--	--
F3	0.67	0.65	0.97	0.054
F4	0.38	0.30	0.79	0.028
F5	0.87	0.86	0.99	0.070
F6	0.74	0.70	0.95	0.058
F7	0.47	0.40	0.85	0.035
F8	0.35	0.20	0.57	0.022
G1	0.40	0.29	0.73	0.028
G2	0.53	0.44	0.83	0.039
G3	0.68	0.64	0.94	0.054
G4	0.70	0.67	0.96	0.056
G5	0.88	0.85	0.97	0.070
G6	--	--	--	--
G7	0.62	0.60	0.97	0.049
G8	0.74	0.74	1.00	0.060
H1	0.74	0.71	0.96	0.059
H2	0.84	0.82	0.97	0.067
H3	0.53	0.48	0.91	0.041
H4	0.30	0.21	0.70	0.021
H5	0.37	0.31	0.84	0.028
H6	0.45	0.42	0.93	0.035
H7	0.57	0.57	1.00	0.046
H8	0.70	0.68	0.97	0.056
J1	0.61	0.53	0.87	0.046
J2	0.63	0.55	0.87	0.048
J3	--	--	--	--
J4	0.70	0.65	0.93	0.055
J5	0.69	0.64	0.93	0.055
J6	0.76	0.72	0.95	0.060
J7	0.72	0.71	0.99	0.058
J8	0.65	0.61	0.94	0.051
J9	--	--	--	--
J10	--	--	--	--
J11	--	--	--	--

TABLE 7 (cont.)

Weld No.	Bead Width (cm)		Ratio	Nugget Area
	Front, d_f	Back, d_b	d_b/d_f	(cm^2)
K1	0.42	0.28	0.67	0.028
K2	0.53	0.46	0.87	0.040
K3	0.63	0.58	0.92	0.049
K4	0.73	0.68	0.93	0.057
K5	0.43	0.32	0.74	0.030
K6	0.54	0.52	0.96	0.043
K7	0.61	0.55	0.90	0.047
K8	0.64	0.61	0.95	0.051
K9	0.38	Incomplete penetration		--
K10	0.54	0.51	0.94	0.043
L1	0.71	0.71	1.00	0.058
L2	--	--	--	--
L3	0.34	0.17	0.50	0.021
L4	0.56	0.53	0.95	0.044
L5	0.33	0.20	0.61	0.021
L6	0.37	0.26	0.70	0.025
L7	0.46	0.41	0.89	0.035
L8	0.53	0.49	0.92	0.041

TABLE 8

HEAT TRANSFER EFFICIENCY FOR THE FULL PENETRATION WELDS

Weld No.	H ($cal.cm^{-1}$)	H_{net} ($cal.cm^{-1}$)	μ_1
F3	515.3	288.1	0.56
F5	568.4	357.6	0.63
F6	515.2	312.7	0.61
G4	488.7	299.5	0.61
G5	572.8	358.0	0.63
G7	452.4	272.5	0.60
G8	527.96	312.7	0.59
H1	486.0	312.7	0.64
H2	528.5	345.8	0.65
H7	453.2	256.0	0.56
H8	496.8	299.0	0.60
J6	489.0	318.4	0.65
J7	489.0	305.6	0.62
K6	435.7	246.6	0.56
K8	488.6	278.7	0.57
L1	389.9	269.3	0.69
L4	341.3	219.2	0.64

TABLE 9

RATES OF HEAT INPUT DURING HIGH PULSE TIMES OF SELECTED WELDS, CALCULATED BY ASSUMING Q (t_b) = 0

Weld No.	Q During t_p ($cal.s^{-1}$)
F3	2827
F8	2827
G1	1988
G5	4538
J4	3918
J6	3918
J7	3918

TABLE 10

COMPUTED RATES OF MOVEMENT OF SOLID LIQUID INTERFACE FOR THE WELD NO. J-7

Time Elapsed After $i_p \rightarrow i_b$ Transition (ms)	Rate (R_t) Transverse to Weld Axis ($mm.s^{-1}$)	Rate (R_w) Along the Weld Axis ($mm.s^{-1}$)
90	5.55	2.12
130	3.85	2.12
230	3.85	2.12
330	3.85	5.98
430	3.85	13.65

TABLE 11

A LIST OF H, H_m AND μ_2 VALUES FOR THE WELDS

Weld No.	H ($cal.cm^{-1}$)	H_m ($cal.cm^{-1}$)	μ_2	Comments
F1	298.7	--	--	Incomplete penetration
F2	614.5	--	--	Burn through
F3	515.3	137.4	0.27	
F4	382.7	70.8	0.18	
F5	568.4	180.2	0.32	
F6	515.2	150.0	0.29	
F7	383.0	90.6	0.24	
F8	342.6	57.3	0.17	
G1	358.5	71.9	0.20	
G2	420.0	101.1	0.24	
G3	488.7	137.5	0.28	
G4	488.7	146.7	0.29	
G5	572.8	180.2	0.31	
G6	625.5	--	--	Burn through
G7	452.4	127.1	0.28	
G8	527.9	154.2	0.29	
H1	486.0	151.1	0.31	
H2	528.5	172.9	0.33	
H3	*	105.2	--	
H4	321.3	53.1	0.16	
H5	369.9	70.8	0.19	
H6	408.2	90.6	0.22	
H7	453.2	118.8	0.26	
H8	496.8	143.8	0.29	
J1	489.0	118.8	0.24	
J2	489.0	122.9	0.25	
J3	489.0	--	--	Burn through
J4	489.0	140.6	0.29	
J5	489.0	138.6	0.28	
J6	489.0	154.2	0.31	
J7	489.0	149.0	0.30	
J8	472.3	131.3	0.28	
J9	625.6	--	--	Burn through
J10	449.0	--	--	Burn through
J11	392.0	--	--	Burn through

TABLE 11 (cont.)

Weld No.	H ($cal.cm^{-1}$)	H_m ($cal.cm^{-1}$)	μ_2	Comments
K1	382.9	72.9	0.19	
K2	436.3	103.1	0.24	
K3	488.8	105.2	0.21	
K4	541.0	146.9	0.27	
K5	382.6	78.1	0.20	
K6	435.7	110.4	0.25	
K7	488.5	120.9	0.25	
K8	488.5	130.2	0.27	
K9	244.4	--	--	Incomplete penetration
K10	341.4	109.4	0.32	
L1	389.9	147.9	0.38	
L2	389.8	--	--	Burn through
L3	244.2	53.1	0.22	
L4	341.3	113.6	0.33	
L5	238.6	55.2	0.23	
L6	238.7	65.6	0.27	
L7	272.7	90.6	0.33	
L8	318.5	106.3	0.33	

* i_b = 5A was too low to determine arc voltage (Figure 4).